ΠΟΛΥΤΕΧΝΕΙΟ
ΚΡΗΤΗΣ /
TECHNICAL
UNIVERSITY
OF CRETE

Electromagnetic Analysis and Condition Monitoring of Induction Motors

Thesis by

Adrián Martín Marrón

Supervised by

Dr Konstantinos Gyftakis

In Partial Fulfillment of the Requirements for the
Degree of
Industrial Electronics and Automation Engineering

TECHNICAL UNIVERSITY OF CRETE
Crete, Greece

2025
Defended 9/07/2025

ACKNOWLEDGEMENTS

I would like to express my sincere thanks to all those individuals and institutions that have contributed so significantly to the elaboration of this dissertation.

Firstly, I would like to express my gratitude to my tutor, Dr Konstantinos Gyftakis, for his invaluable guidance, time and valuable suggestions throughout the work. In addition, I would also like to extend my gratitude to Professor Daniel Moriñigo Sotelo, whose help has been essential for the successful completion of this work at the Technical University of Crete.

Finally, I would like to express my gratitude to my family for their constant support and for offering me the necessary conditions to carry out this formative stage.

To all of them, my sincere gratitude.

ABSTRACT

The present thesis outlines the design, modelling and electromagnetic analysis of a squirrel-cage induction motor under both healthy and faulty conditions. The development of a two-dimensional geometry was undertaken using AutoCAD software, and consequently, a two-dimensional simulation was conducted utilising SIMCENTER MAGNET, incorporating the Finite Element Analysis (FEA) method. Numerous diagnostic techniques—such as Motor Current Signature Analysis (MCSA), Stray Flux Signature Analysis (SFSA), and Short-Time Fourier Transform (STFT)—were employed to determine the motor's response in both star and delta configurations. The study focuses on identifying and comparing the effects of rotor bar faults, with the objective of check the efficiency of these preventive techniques. The results demonstrate that electromagnetic simulation combined with signal processing techniques provides a powerful tool for early fault detection in industrial motors.

TABLE OF CONTENTS

LIST OF ILLUSTRATIONS

LIST OF TABLES

NOMENCLATURE

Analysis terms.

FEA. Finite Element Analysis.

FFT. Fast Fourier Transform.

MCSA. Motor Current Signature Analysis.

SFSA. Stray Flux Signature Analysis.

STFT. Short Time Fourier Transform.

Electrical terms.

AC. Alternating Current.

EMF. Electromotive Force.

HV. High Voltage.

IM. Induction Motor.

LV. Low Voltage.

RMF. Rotatin Magnetic Field.

RMS. Root Mean Squared.

Physics Constants.

ε_0**.** Electrical constant.

μ_0**.** Magnetic Permeability.

Chapter 1

INTRODUCTION

1.1 Background and Motivation [1], [2]

Today's society is highly dependent on energy, either directly or indirectly. This is a basic need, but at certain times it can lead to high economic expenditure, for example in industrial processes. As a result, there is a need for improvement in the efficiency and quality of electrical machines in these processes.

Although many types of electrical machines can be used in low power industrial applications, depending on the needs of the system, a thorough market research shows that the vast majority of industrial motors are still induction motors, which makes their study a crucial step in the development of the industry.

Induction motors are often referred to as the workhorses of industry due to their robustness, reliability and simplicity. This makes them extremely versatile and useful in a wide range of industrial applications. They are used extensively in a variety of sectors, including the manufacturing, transport and energy industries. Their essential role in industrial processes makes it vital to ensure their optimum performance and reliability.

Consequently, monitoring and controlling such engines throughout their normal operation, or abnormal operation caused by faults, has become an essential task in engine design. Firstly, early detection of faults such as rotor bar breakage, stator winding defects, unbalanced voltages or bearing wear can reduce the cost and lead time of motor maintenance, making them more efficient and cost-effective. This fault detection is done by creating a threshold when the machine is operating under normal conditions. This threshold serves as a precedent to identify when the machine is operating under abnormal conditions.

Secondly, studying the engine when it is operating under abnormal conditions serves as a source of data for the creation of predictive software that will aid in the early detection of faults. These monitoring techniques and software range from engine vibration analysis or a motor current signature analysis (MCSA), to engine thermal analysis, helping to detect problems before they lead to irreversible engine damage.

It is also important to note the importance of the connections used in the motor circuit and the derived motor behaviour. These two connections, delta and star, are the ones that determine

how the motor will start, operate and respond to the load[1] variations that occur.

In the star configuration, the motor receives a reduced voltage, which limits the inrush current during start-up. This makes it ideal for applications requiring a soft start. In contrast, the delta configuration allows the motor to operate at full mains voltage, providing higher torque and efficiency once the motor is running.

Understanding the different electrical and mechanical characteristics of the two connections enables engineers and designers to:

- Optimise start-up procedures and energy consumption.
- Assess motor performance under different load and voltage conditions.
- Detect faults that may only manifest under specific configurations.
- Design more effective protection and control systems.

All these studies and analyses have resulted in these motors obtaining a reduced energy cost, an increase in service life and a confirmation of continuity in industrial processes. All these improvements have led to the development of induction motors, and therefore of electric machines, to a great extent, making numerous advances capable of helping society.

As in the case of transformers, a type of electrical machines, where their development has allowed the transport of electrical energy over long distances has been developed to a great extent and in a crucial aspect.

1.2 Objectives and Methodology

The objectives of this thesis mainly concern the design, modelling, and later analysis of a squirrel-cage induction motor. The analysis will mainly compare the different case studies of healthy and failed engines and the differences between the two possible connections of the induction motor, star and delta. The methodology followed in this thesis can be summed up into these points:

- Design of the 2D motor's outline through the design software AUTOCAD.
- 3D modelling, electromagnetic extension and simulation of the induction motor model by the FEA resolution software SimcenterMAGNET in different study cases (Healthy and faulty ones).

[1] The so-called loads are those referring to any element that consumes power.

- Obtaining measurements of voltage, current, motion and magnetic flux (By three sensors placed on the motor) of the different simulations using a sampling frequency of 10KHz.
- Treatment and analysis of the measurements including a current, torque and STFT study using MATLAB software.
- Compare and observe the results given by the analysis and detect the main anomalies between the different connections and the different study cases of the motor, providing a good point of view to study their impact.

1.3 Finite Element Analysis

Finite element analysis, or FEA, is a numerical technique used in engineering due to its diversity and flexibility as an analysis tool. This method takes all the complexities of the problems, like varying shape, boundary conditions or loads, and maintains them as they are, while the solutions provided by it are approximate [3]. This method has boosted the development of many computer hardware and software, since computers are the only devices that can support this type of analysis.

On real models, there exist infinite complexities called field variables or unknown elements which can not be calculated or even estimated. These unknown variables can be solid mechanics, velocity in fluid machines or electric and magnetic flows. The finite element analysis procedure reduces this field variables into smaller ones, called elements, to proceed with express the unknown variables into approximated functions.

This technique mainly differs with respect to the classic techniques in three aspects: the made assumptions, the obtained results and the non-linearity in the models. Regarding the first point, the classic techniques make assumptions drastically, whereas the FEA doesn't make any, so although the problem is more complex, it provides more accurate values. Regarding the second point, while the classic techniques search for exact results to their problems, the FEA is only responsible for search approximations. Regarding the third and last point, the FEA can confront problems that include materials and geometries non-linear, whereas the classic ones are only able to focus on linear problems [4].

Mathematical Background

The solution to the finite element analysis (FEA) problems is found by solving Maxwell's equations under given boundary conditions. The differential equations delineated in this section establish the fundamental principles that govern finite element analysis (FEA) boundary-value problems. This set of equations, Maxwell's laws, is responsible for describing all

macroscopic electromagnetic effects. For a better understanding of this analysis, these equations are expressed in differential form, although they can also be expressed in integral form, as will be seen later.

The differential form of Maxwell's equations can be derived by applying the Gauss and Stokes theorems. The theorems facilitate the expression of the integral expressions of these laws in terms that can be related to points in space where the values of the fields and their derivatives are continuous.

The Maxwell equations in their derivative form are as follows:

Faraday's law

$$\nabla \times E = -\frac{\partial B}{\partial t} \tag{1.1}$$

Maxwell-Ampere Law

$$\nabla \times H = \frac{\partial D}{\partial t} + J \tag{1.2}$$

Gauss's Law

$$\nabla \cdot D = \varrho \tag{1.3}$$

Gauss's Law - Magnetic Field

$$\nabla \cdot B = 0 \tag{1.4}$$

Equation of Continuity

$$\nabla \cdot J = -\frac{\partial \varrho}{\partial t} \tag{1.5}$$

The symbol E is employed to denote the electric field strength, whilst D is used to denote the electric flux density. The symbol H refers to the magnetic field strength, B denotes the magnetic flux density, J is used to denote the electric current density, and ρ is used to denote the electric charge density.

The analysis solves these equations by reformulating their first-order form, which involves two field magnitudes, into second-order equations involving only one field magnitude. Once these expressions have been obtained, specific boundary conditions are assigned to them, depending on the problem, with the objective of obtaining an approximate solution to the original

Implementation Via Software

In the field of finite element analysis (FEA), simulation analysis can be approached in two distinct ways: either a linear or a non-linear method. These approaches depend on the material

properties that make up the problem as well as the complexity of the problem. Utilising a linear approach, the simulation software employs a fixed relative permeability value for each material, which is defined by the user. However, if a non-linear approach is employed, the simulation software incorporates the B-H curves of the material, providing more accurate values for the magnetic saturation effect of the material.

The following list outlines the key steps involved in the implementation of the FEA for MI analysis.

1. **Geometry definition**: This step proceeds with the model's geometry design, which can be in 2D or 3D depending on the analysis to make.

2. **Mesh generation**: In this step we proceed with the division of the problem domain into a mesh for each element to be analysed. It is in this mesh where the different finite elements to be solved will be found. The form of these elements depends on the analysis to be carried out. For 2D analysis, these elements are usually triangular or quadrilateral, while for 3D analysis, tetrahedral or hexahedral elements are more commonly used.

3. **Solver execution**: In this step, the solver assembles and solves the system of equations generated on the mesh. These solvers can be direct, iterative, non-linear,... The SIMCENTER MAGNET software, which is the one used in this thesis, makes use of Newton Raphson.

4. **Post processing**: As a final step, this is where data is post-processed once it has been collected, so that it can be made more accurate and accessible for further studies.

In the second step, the meshes elaborated are those entrusted with the control of the accuracy with which the problem is solved. The size of the elements it produces is a critical step in the outcome of this analysis. When a small mesh is generated, where its elements are consequently also small, more accurate values are obtained. However, this comes at the cost that the computational load will increase by a large average. This principle behind mesh refinement dictates that for more accurate results, the density of these meshes must be increased.

Collectively, these steps constitute the workflow necessary for the correct execution of FEA in the analysis of induction motors, thus ensuring that the results obtained are both valid and accurate.

1.4 Outline

Chapter 1 Introduction: This chapter provides an overview of the thesis, including the background that flashed the interest in this topic, the objectives of the research, the methodology employed, and a summary of each chapter included in the thesis.

Chapter 2 Theoretical Background: This chapter offers general knowledge about electrical machines, their base and how they are divided into different groups. This explanation will be general and will be the base for the rest of the chapters.

Chapter 3 Modelling setup: This chapter explains how the model has been built, offering the different steps followed and a detailed description of each component present in it.

Chapter 4 Study cases and simulations: This chapter offers the results of the simulations made on the thesis, including explanations and comparisons with the different models. This chapter contains the main part of the thesis.

Chapter 5 Conclusion and future work: This chapter offers the final sum up of the thesis and a small list of ideas to improve the work or continue it to make it better.

Chapter 2

THEORETICAL BACKGROUND [5]

This chapter will discuss the basis of the induction motor under consideration. In the first place, it will be spoken about the general bases of the electrical machines, to jut out later on more specific information about the different types of these machines. Finally, an explanation will be given of the exact type of motor used in this thesis, leaving the specific values of its composition to the next chapter.

2.1 Electrical Machines and Electrical Conversion

For mankind, energy conversion has always been a crucial process in its development, being present at all times in daily life. Because of this fact, from the Industrial Revolution to the present day, the need for efficient electromagnetic energy conversion has been gaining exponential importance, to the point of having to develop and discover machinery to satisfy such needs. These machines are the so-called electric machines[6].

Electrical machines are devices that allow the conversion of energy, on the first moment electrical energy, to a different type and vice versa. This conversion takes place inside the machine, where electrical and magnetic circuits are located. Within these devices, also there are ones that transform electrical energy changing its properties only, resulting in the same type of energy but with different characteristics, that will be necessary for later use.

The theoretical grounding of this type of machine is based on electromagnetism. This science branch studies how electrically charged particles interact with electrical and magnetic fields. Many factors are capable of affecting the characteristics of these magnetic fields, thus modifying their size and direction. These factors can be the intensity and direction of the current flowing through the wire, the distance between the measuring point and the wire as well as the shape of the wire.

To begin with, it is necessary to distinguish two different types of magnetic field, the static and the variable[1] ones. The static magnetic fields, the ones that will be studied on this thesis, are the ones produced by constant charge movement like electrical currents or permanent magnets, whereas the variable ones are produced by a discontinuous charge movement with alternating current. This second type can be distinguished measuring whether or not the field induces current.

[1] The variable term refers to the time and radiation of the field

In order to study these magnetic fields, it is necessary to know their direction and sense, therefore the rule of the right-hand is used, as shown in Figure 2.1. This rule is a method to determine the vectorial directions and has as its basis the Cartesian planes. The most common use for this rule is to determine the direction of the resulting vector on a vectorial product, but in this area, it allows us to know, based on the direction of the current, how the sense of the electromagnetic field.

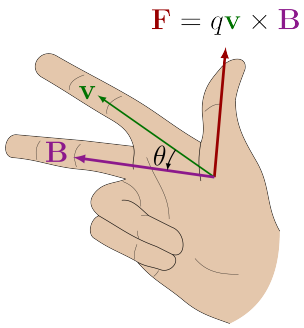

Figure 2.1: Right-hand rule showing the directions of the magnetic field, the tangential speed of the movement and the direction of the electromagnetic force

Once the direction of the magnetic field has been studied, it can be proceed with analysing the effects and phenomena it generates. The most well-known study case is with a straight wire, where, when an electric current circulates through it, it generates both an electric field and a magnetic field around it. The magnetic field corresponds with a circular field that is perpendicular to the wire. The movement of electric charges, along with the creation of the fields, gives rise to one of the best-known phenomena in electromagnetism: the electromagnetic force. This force corresponds to one of the four fundamental forces of the universe and is responsible for attracting more electric charges, leading to an increased movement of particles. This attraction only occurs if the particles are within the range of action of the electromagnetic field.

A very curious effect of this force is produced in the case of a rectangular spiral wire, such as the one shown on the Figure 2.2, where the appearance of this force causes a movement of the conductor wire. In this case, the shape of the wire causes two electromagnetic force vectors, of equal magnitude but opposite direction, to be generated at the ends of the wire. This pair of forces is responsible for making the wire start to rotate around itself.

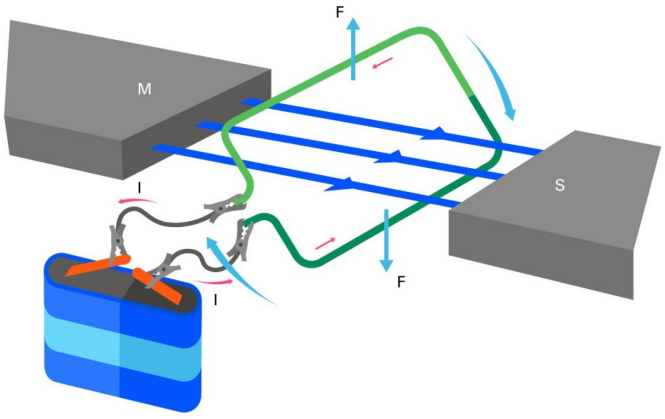

Figure 2.2: Electromagnetic force in a rectangular spiral [7]

This phenomenon, caused by the rectangular spiral, serves as a precedent for the development of numerous devices, capable of taking advantage of the movement caused and creating an attempt to convert energy more efficiently.

2.2 Electromagnetic Laws

All of these phenomena previously mentioned are determined by different laws that rule the electromagnetic field's behaviour. The most important laws and the ones that are important to know are Faraday's law, Ampere's law, and Gauss's law.

This laws will be necessary to distinguish numerous types of electrical machines depending on how they are built, what is their type of current and how they get excited. This classification can be observed on Figure 2.3 below.

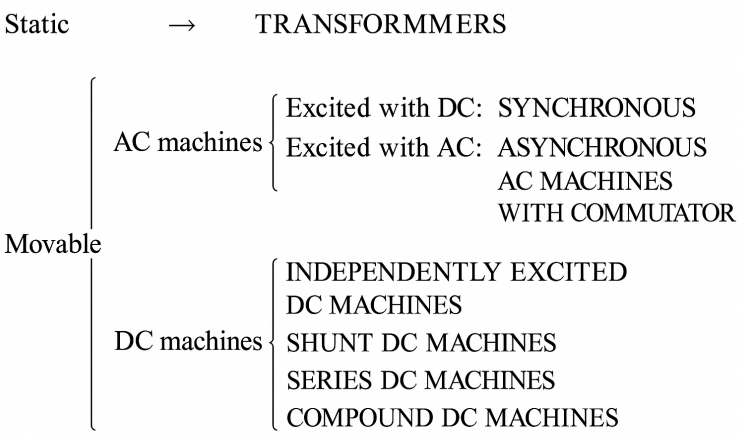

Figure 2.3: Classification of the electrical machines [8]

To understand better these laws, is important to have some knowledge about some terms like the electromotive force and the magnetic flux. The electromotive force, or EMF, is the difference in potential that occurs between two points when an electrical charge moves between them. In more exact terms, this EMF is the origin of the separation of charges with different signs between their electrodes and therefore the cause of a constant potential difference between their electrodes.

Furthermore, the magnetic flux corresponds with a measurement way of the magnetic field for quantify how much of this field pass along a close surface. This flux allows to calculate how much magnetism exists on a determinate point.

Ampere's Law (1826)

The Amperes' law, formulated on 1826 by the French scientist André-Marie Ampère, constitute an essential step on the electromagnetism development. This law is the one entrusted on make the relation between the density of the static magnetic field created and the stationary electric current. In other words, this law provides an explanation of how increasing the current flowing through a conducting wire increases the density of the magnetic field, thus making it clear that there is a direct proportionality between these parameters. This relationship can be seen in the following equation:

$$\oint \mathbf{B} \cdot d\mathbf{l} = \mu_0 I \tag{2.1}$$

where B refers to the density of the magnetic field, dl refers to the derivate of the length on the conducting wire, μ_0 refers to the magnetic permeability[2] of the space and finally I refers to the current that pass trough the wire.

Later, this law will be corrected by the scientist James Clerk Maxwell, making it part of one of Maxwell's laws and making it one of the pillars of electromagnetism in classical physics.

Faraday's Law (1831)

In 1831, Michael Faraday made a groundbreaking contribution to science with his discovery of electromagnetic induction, formulating the law that later will have his surname. This law describes the magnitude of the EMF induced in a wire due to the electromagnetic induction caused. This rule makes the relation of the speed of the flux of time change on a close surface and the inductive voltage on the circuit. In easier terms, describes how an electromagnetic

[2]Its purpose is to quantify the strength of the magnetic field emitted by an electric current.

change can produce energy. This relation is shown in the equations below:

$$\varepsilon = -N\frac{d\Phi_B}{dt} \tag{2.2}$$

$$\Phi_B = BA\cos(\theta) \tag{2.3}$$

where the ε refers to the induced EMF, N is the number of turns on the coil, Φ_B to the magnetic flux, B is the magnetic flux density, A is the surface area and θ is the angle between the magnetic field vector and the normal vector to the surface.

Lenz's Law (1833)

As a direct consequence of Faraday's law, in 1833, Henrick Lenz formulated a series of rules and reasoning on how to determine the direction of the current induced in the conductor wire by the EMF. By means of numerous experiments, Henry observed and came to the conclusion that this current produces a magnetic field, which tends to oppose the change in the magnetic flux that induces such currents.

To observe this behaviour graphically, it is only necessary to carry out a small experiment with a close conductor wire and a magnet, according to Figure 2.4. While the magnet is in movement, it will generate an EMF on the close wire according to the equation 2.2, inducing a current. Now, to determine the direction of the current will use the right-hand rule, placing the thumb on the positive direction of the vector A, and curling the rest of the fingers around the closed loop. If the EMF is positive, the induced current will follow the direction of the fingers, meanwhile, if it's negative, it will be in the opposite direction. All of the possible situations are summarized in the table below.

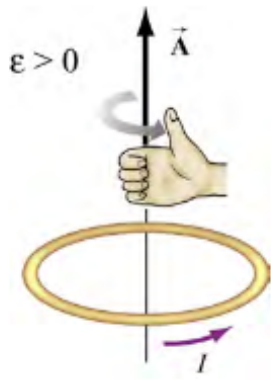

Figure 2.4: Experiment used to prove the Lenz's law with the right-hand rule [9]

Φ_B	$d\Phi_B/dt$	$\mathcal{E}$	I
+	+	−	−
+	−	+	+
−	+	−	−
−	−	+	+

Table 2.1: Relationship between magnetic flux, its change over time, induced emf, and the direction of the current induced [9]

Gauss's Law (1835)

In 1835, by the direct hand of the scientist Carl Friedrich Gauss, the Gauss' law was formulated. This law, with has strong relation with the divergency theorem, make a direct relation between the flux of the electromagnetic field trough a close surface and the magnitude of the charges that are inside that surface. In simple words, it refers that the net flux of the through any hypothetical closed surface is $\frac{1}{\varepsilon_0}$ times the net electrical charge enclosed on the same surface. This relationship can be seen in the following equation:

$$\Phi_E = \frac{Q}{\varepsilon_0} \tag{2.4}$$

where Φ_E refers to the electric flux trough the closed surface, Q refers to the enclosed electric charge on the surface and finally ε_0 refers to the electrical constant[3].

Halls' Effect (1879)

Although the Hall effect is not strictly speaking a law, it is worth naming it to understand certain explanations that will be given in this thesis.

Discovered in 1879, the Hall effect describes the phenomenon where an electric field is generated due to a charge separation within a conductive wire, where a current passes through the presence of a magnetic field. Linked to this electric field generated appears the so-called Hall voltage, which is the potential difference measured between the two edges of the wire. Hall voltage is strongly related to the magnetic field that produces it, as it can be seen in equation 2.5 shown below.

$$V_H = Blv_d. \tag{2.5}$$

In this equation, the term B represents the magnetic field density, l denotes the length of the wire and v_d refers to the electron drift velocity.

[3]It is a measure of the density of an electric field formed in a vacuum in response to the presence of electric charges.

Since its discovery, the Hall effect has been used to investigate electrical conduction in various materials: conductors, semiconductors, and electrolytic solutions. Due to the establishment of this relationship, it has been possible to develop sensors that measure the electrical voltages produced in induction motors, thus helping to increase their development.

2.3 Losses and Undesired Effects [10], [11]

It is important to know that these electrical machines do not perform energy conversion in an ideal way; on the contrary, certain losses occur during the process. These energy losses cause the electrical machines to not work with perfect efficiency and thus impair their performance, so understanding and mitigating them is crucial for improving the performance and longevity of these motors.

The effects and phenomena that cause these losses can be mainly due to Foucault currents (edgy currents) or hysteresis losses, among many others.

The first phenomenon, edgy currents, is an electrical phenomenon discovered by the French physicist Leon Foucault in 1851. These currents can be demonstrated by observing that in electromagnetism, the induced currents don't have an ideal behaviour. Until now, ideal examples have been assumed where the induced current in the conductor is obliged to follow the conductor's trajectory, whereas, in reality, these conditions are not present. In the presence of a real conductor wire, which is in motion within a magnetic field, or when there is a variable magnetic field, certain currents are induced which circulate through the conductor's volume. These currents dissipate energy in the form of heat, resulting in a significant efficiency loss.

The second phenomenon to be considered is hysteresis, a magnetic phenomenon with electrical implications, particularly with regard to induction motors. It occurs when ferromagnetic materials cannot cope with rapid variations in the applied magnetic field, which prevents them from immediately returning to their original state and leads to residual magnetism.

This delay in the magnetism of the material impacts the performance of induction motors in multiple ways. Firstly, magnetic losses decrease the machine's efficiency and reduce the torque produced at low speeds, while increasing energy losses. Secondly, the energy lost due to hysteresis is converted into heat, which can cause the operating temperature of the motor to increase, resulting in the machine elements degrading more rapidly.

2.4 Static Electrical Machines

Static machines, or transformers, are electrical devices that modify the characteristics of the electrical energy supplied to them, increasing or decreasing the amplitude of the voltage but maintaining the operating frequency. Their design can be simplified with three main components: two alternating current windings wound on a magnetic core, as shown in Figure 2.5 below.

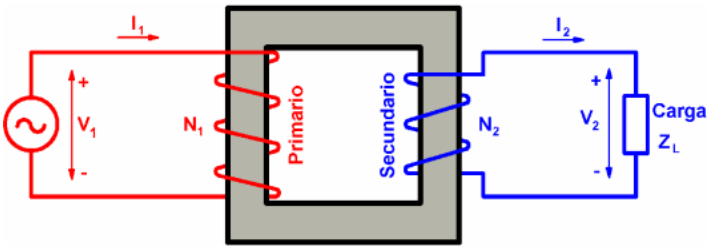

Figure 2.5: Working principle of a single-phase transformer [8]

Composition and Operation Principle

The core is the centre of the transformer and is its most important component. The one shown in the Figure above corresponds to a core made up of overlapping electromagnetic sheets without an air gap, although it can be also created by solid steel. This component has the function of contain the electromagnetic flux produced by the windings, therefore it also reduce the significative loss due to the Foucault currents.

The primary winding is the winding through which energy enters, while the secondary winding is the winding through which energy exits to feed the loads. Using the schematic as a starting point, the operation of a transformer can be explained as follows. When the primary winding is supplied with an alternating voltage V_1, an alternating flux is generated in the magnetic core. This flux, by means of Faraday's law explained previously in the equation 2.2, induces an electromotive force which gives rise to a voltage V_2 between the terminals of the secondary winding.

It should be noted that transformers are reversible machines, which can be used to reduce the amplitude of a voltage if they are supplied from the HV side, or increase it if they are supplied from the LV side.

Analysis of the Equivalent Electrical Circuit

In order to analyse the operation of this type of machine in more detail, an equivalent circuit is used to characterise the different elements of the transformer. This circuit can be seen in the Figure 2.6 and it is thanks to it that the different currents and voltages present in the

machine can be calculated. This circuit shows the three main parts mentioned above, the primary winding on the left, the magnetic core in the centre, and the secondary winding on the right.

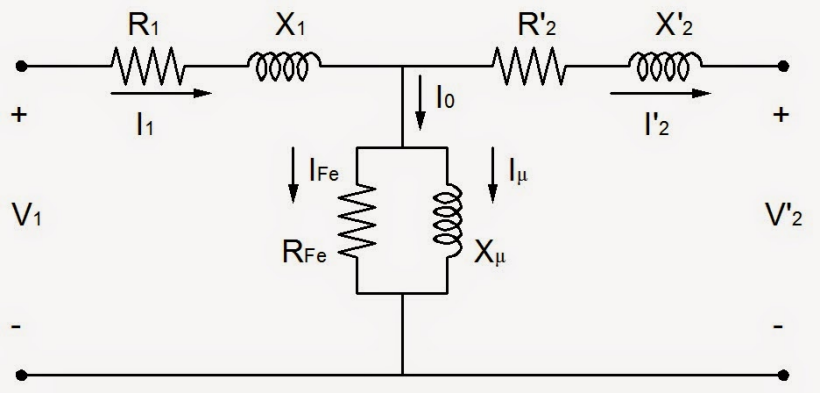

Figure 2.6: Equivalent circuit of a single-phase transformer [12]

The main components of this circuit are the followings one:

- R_1: Ohmic resistance of the stator winding which is responsible of the copper losses of the stator windings.
- R_2: Rotor resistance, which is responsible of the joule losses[4] of the rotor.
- X_1: Stator leakage reactance.
- X_2: Rotor leakage reactance.
- X_μ: Magnetising reactance.
- R_{Fe}: Core losses.

These components make it possible to calculate the conversion ratio of the machine, which is crucial for understanding and developing the various methods used to analyse the transformer, such as the primary method. This relationship is defined by equation 2.6, which establishes a relationship between the number of turns in the windings and the voltages and currents passing through them.

$$m = \frac{N_1}{N_2} = \frac{V_{1N}}{V_{2N}} = \frac{I_{2N}}{I_{1N}} \tag{2.6}$$

[4]Electric energy converted in heat by the resistive losses irreversibly

The primary method is the most commonly used approach for analysing all components of the transformer. This method involves adapting the elements related to the secondary winding and modifying them to create a new winding with the same number of turns as the primary winding. Mathematically, this adaptation assumes a variable change that allows for the simplest analysis of the machine.

Using this method enables characteristics such as maximum flux to be maintained at the same value, ensuring the machine's efficiency. The equations relating the different parameters of the secondary winding to the new ones are summarised below:

$$\begin{aligned} \overline{V}_2' &= m\,\overline{V}_2 \\ \overline{I}_2' &= \frac{\overline{I}_2}{m} \\ Z_L' &= \frac{V_2'}{I_2'} = m^2\,Z_L \\ R_2' &= m^2\,R_2 \\ X_2' &= m^2\,X_2 \end{aligned} \tag{2.7}$$

2.5 Rotative Electrical Machines

Rotating machines constitute the second major group of electrical machines. In contrast to the static machines previously discussed in section 2.4, these machines are based on the rotation of the moving components that they are composed of. This makes it possible to differentiate between two elements in this type of machine: the stator and the rotor.

The stator, on the one hand, corresponds to the fixed component of the machine, which is made up of a magnetic core to which the different windings are attached. The material used to construct the magnetic core is typically ferromagnetic, most often silicon steel plate, with the objective of minimizing losses due to parasitic currents. The component under consideration typically assumes the form of a hollow cylinder, which serves to contain the moving component.

On the other hand, there is the moving component of the machine, the rotor. This element is located inside the stator and is built with the same magnetic core as the stator. This core is formed in such a way that it can hold both windings and busbars, the distinction being dependent on the sub-type of the rotating machine. As with the stator, this component is typically composed of a hollow cylinder. This design facilitates the accommodation of the machine shaft or the machine tree, which can be housed within and affixed to the component.

The two elements, despite being enclosed within each other, do not come into direct contact. On the contrary, there is a minimum separation between whose function is to avoid collisions

between them, the frictional force and the losses associated with it. This separation is referred to as the "air gap," and it is the space within which the primary electromagnetic effects occur during the machine's operation.

When talking about the aforementioned windings, they do not necessarily always have to be in the stator. They can be located along the perimeter of both the stator and the rotor, housed in small slots. Their location will depend on the type of rotating machine in question, and therefore on the principle of operation required.

These types of rotating machines can be divided according to the type of current they handle, being either alternating current (AC) machines or direct current (DC) machines.

DC Machines

This particular type of rotating machine is powered by a direct current source in both induced winding[5] and inductor winding[6]. In contrast to AC machines, this devices posses a fixed polarity and no frequency, which makes them more useful in low-power, short-distance applications, where easier speed management is required for changes in flow or voltage. Regardless of this, these types of machines have the disadvantages of being more complex than AC machines and more expensive, which makes them a difficult task to maintain and repair. The construction of these machines can be summarised as follows: the inductor winding is in the stator and the induced winding is in the rotor.

It is important to note that in this particular type of machine, the magnetic core of the rotor is created by stacking magnetic plates in order to mitigate the magnetic losses produced by the variable magnetic field to which it is subjected. On the other hand, the magnetic core of the stator, being under the effect of a static magnetic field, is made of solid iron, since the magnetic losses in it are almost non-existent.

In reference to the principles of operation of these machines, they can be categorized as either a motor or a generator, depending on how the inducted winding is supplied. In case the machine works as a motor, this winding is supplied with DC. Consequently, when it interacts with the magnetic field created by the inductor, an EMF is produced, which in turn generates a torque capable of rotating the rotor. This is a similar case to the one shown in the Figure 2.2. Meanwhile, when the machine functions as a generator, it must be supplied with mechanical energy by a motor coupled to the shaft of the machine. This will result in the movement of the coils within the inductor's magnetic field, which, according to Faraday's

[5]Moving part where the current is induced or circulated.

[6]Fixed part generating the magnetic field.

law, will generate an EMF capable of inducing an electric current to the outside, as long as it is in a closed circuit (connected to a load).

The classification of these electrical machines can also be based on the manner in which the inductor and the induced windings are connected. This results in a multitude of possible configurations, including independent excitation, in series, shunt, or compound.

AC Machines

In this type of rotating electrical machines, two subtypes can be distinguished, those that are excited by DC (synchronous machines) and those that are excited by AC (asynchronous machines). The first type will be discussed in this section while the other type will be explicated in more detail below.

Synchronous machines, or AC machines excited by DC, are a subtype of electrical machines where the inductor winding is in the rotor and the induced winding is in the stator, unlike DC machines. In the case of the rotor, it is supplied by DC with a two-ring collector[7], whereas the stator's windings are made to withstand AC. In this type of machines, the magnetic core of the stator is built by staking magnetic sheets.

The distinguishing characteristic of this particular machine is its rotational speed, known as synchronous speed, which gives synchronous machines their name. In order to ensure that the generated voltages maintain a consistent frequency, it is imperative to maintain a constant machine speed. This constant speed can be calculated by utilizing the following equation:

$$n = \frac{60f}{p} \tag{2.8}$$

Where the term f denotes the working frequency of the machine, while p is employed to indicate the number of pole pairs of the machine.

To achieve this synchronous speed there are different ways, because like DC machines, synchronous machines can be used both as motors and generators. In the case of generator operation, the rotor, already being supplied by a direct current, is connected to an external driving machine which rotates both it and the magnetic field attached to it. From the rotor's point of view, the magnetic field remains static, while for the coils housed in the stator, on the other hand, the rotation of the magnetic field is defined as variable, resulting in the stator's coils being subjected to a variable magnetic flux, which induces alternating EMFs in them. Due to this the voltages produced work with frequencies of 50 and 60 Hz [8].

[7]Device that allows the transfer of energy, signals and data between a mobile source to a static one or vice versa

In the other case, when the synchronous machine functions as a motor, instead of connecting a driving machine to the rotor, the stator is supplied with an alternating current source. This causes the stator coils to be under a set of balanced currents, resulting in a rotating magnetic field (RMF). As this field interacts with the inducing magnetic field, the rotor rotates at the same speed.

This type of machine has the great disadvantage that it cannot reach the synchronous speed by itself. Instead, they need to rely on an external driving machine to make them rotate at a speed very close to the synchronous speed until both magnetic fields can engage. This makes synchronous machines start-up dependent at all times, making them more expensive to repair and maintain.

In terms of composition, synchronous machines are composed of two distinct types of rotors, distinguished by their operational speed and the composition of their rotor. These rotors are classified as either cylindrical or outgoing poles, both of them shown in Figure 2.7. The cylindrical rotors are synchronous machines with 2-4 poles, which makes them faster and better for applications in thermal centres. Furthermore, the outgoing pole rotors exhibit reduced velocity due to their larger pole number in comparison to the other type. This makes better their use for hydraulic centres [13]. Due to the high speed and the derivative centrifuge force, this type has rotors with an small diameter and a long axial length.

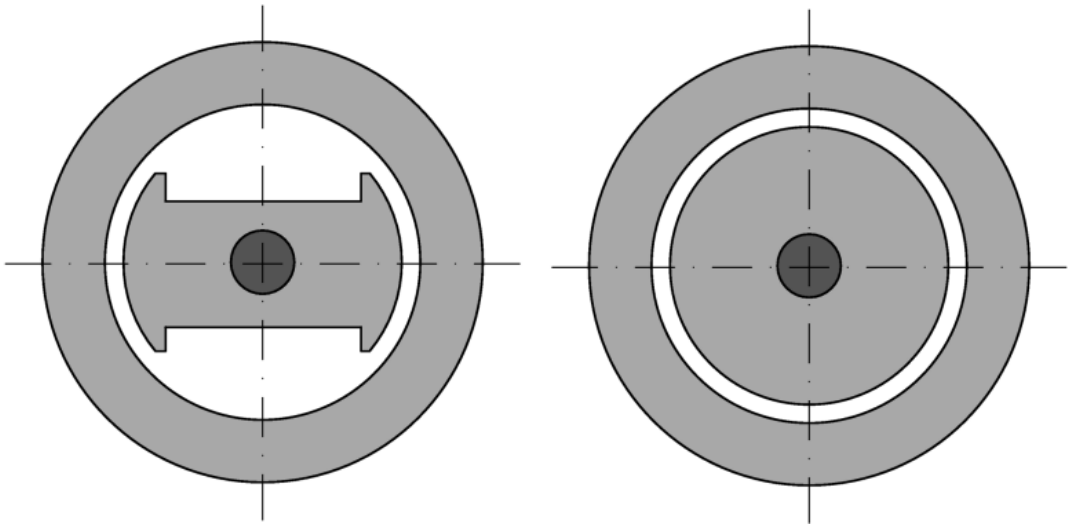

(a) (b)

Figure 2.7: Synchronous motor types depending on the speed which they works: 2.7(a) Outgoing poles and 2.7(b) Cylindrical rotor [8]

2.6 Asynchronous Machines

Asynchronous machines are a category of rotating electrical machines supplied, and also excited, by alternating current. In this type, unlike synchronous machines, the induced winding is housed in the stator while the induced winding is housed in the rotor. Typically, the inductor winding in this type of machine is three-phase, with the exception of small power machines where it can be either two-phase or single-phase. On the other hand, the induced winding is always polyphase.It should be noted that both windings have exactly the same number of poles [14].

As it has been explained in synchronous machines, the magnetic core of which the stator is made is formed by stacking metal sheets.

Operation Principles

The principle of operation of these machines depends on how the magnetic fields responsible for the motion are generated. In this case, the stator is connected to an external source of AC. This current creates a balanced flow in the stator winding, which is responsible for the creation of a RMF. This field then cuts through the rotor bars, inducing AC in them according to Faraday's law. These currents generate a RMF that interacts with the field created by the stator, producing a rotating force in the rotor. Due to the 'induced' nature of the magnetic field in the rotor, the rotation is not synchronous, which means that there is a certain delay in the rotation. This delay is called slip and is calculated using the following equation:

$$s = \frac{n_s - n_r}{n_s} \tag{2.9}$$

where the term n_s refers to the synchronous speed while n_r means the speed of the rotor.

This principle of operation means that this type of machine can operate both as a motor and as a generator. In the case of operation as a motor, which is the most common case, the rotor speed will always be lower than the synchronous speed, because otherwise no torque would be produced. Whereas in the case of generator operation, due to the need to create a braking torque in the machine, the machine has to rotate at a higher speed than the synchronous speed, making an external driving machine necessary for this purpose. This external dependency, together with the increased cost and maintenance involved, means that the generator mode of operation is not widely used.

As a consequence, asynchronous machines are commonly referred to as induction motors (IM), due to their usual mode of operation and the origin of the rotor currents.

Types of Induction Motors

When talking about the composition of these IMs, it should be noted that they can be divided into two main types, depending on how the rotor has been designed, these being: the squirrel-cage motors and the collective-rings motor. Although the object of this thesis is a squirrel-cage motor, both types will be explained to observe their differences.

On a squirrel-cage, the rotor winding is built by a bars made of copper or aluminium. This bars are short-circuited at the upper and lower edges by rings made of the same material as the bars. These short-circuit rings are usually made with protrusions that facilitate heat dissipation in the machine, thus extending its service life. The number of phases of this winding depends on the number of rotor bars to be housed. The squirrel cage rotor is the most commonly used rotor because it hasn't slip rings and therefore it has a longer useful life. Beside this, the production is much cheaper.

In the slip ring motor, on the other hand, the rotor consists of coils instead of rotor bars. These coils are not short-circuited in the rotor, but are guided outwards by slip rings to be short-circuited by additional resistors. The current flow of the rotor can be influenced by the resistors of the electrical machine.

Every difference on both types of rotors are summed up on the table 2.2 below.

	Squirrel-cage	Slip-rings
Advantages	Very cost-effective production Reliable at high-low temperatures High life time	Higher starting torque Low starting current
Disadvantages	Low Starting torque at low speeds Low efficiency High losses on rotor	Additional costs by resistors Unsuitable for high speeds Higher service cost due to slip rings

Table 2.2: Comparison about the advantages and disadvantages between the squirrel-cage rotor and the slip-rings rotor on an induction motor [15]

These features and differences make squirrel cage motors more commonly used in the industrial environment, due to their simplicity, versatility and low maintenance.

Regardless of the type of rotor used, the incorporation of skew angles within rotor slots is a common practice in order to improve the magnetic and mechanical characteristics of the motor. This angle corresponds to the inclination of the rotor slots, where the windings or rotor bars are housed, concerning the longitudinal axis of the motor. This minor alteration in the slot design brings benefits such as a reduction in unwanted harmonics, a smoother starting torque and a decrease in motor noise and vibration. Furthermore, the addition of this

angle causes a more gradual distribution of the magnetic flux in the rods as well as a better current distribution in the rods. Not only is this advantageous, but it is also important, since poor design in this area can lead to increased complexity in winding design, increased stray losses or a slight reduction in maximum torque. Therefore, achieving an optimal balance of the skew angle constitutes a crucial step in the design of these motors.

Equivalent Circuit in Induction Motors

In order to study the behaviour of these motors and analyse the currents and voltages involved, an equivalent circuit has been designed so that all the elements that take part in the normal operation of the machine are shown. This circuit can be seen in the Figure 2.8.

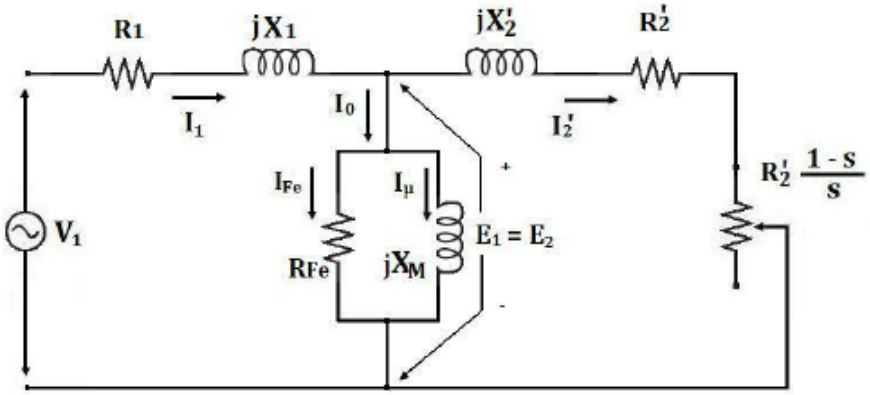

Figure 2.8: Equivalent circuit for a synchronous or asynchronous motor [16]

At first sight it is possible to see the great similarity with the equivalent circuit of the transformers (Figure 2.6), but with an added element: $R'_2 \frac{1-s}{s}$. This variable resistance is not real, but has been created in a fictitious way in order to represent the conversion of electrical energy into mechanical energy in the motor. From an electrical point of view, this resistance models the useful mechanical power before it is lost through friction or other mechanical causes. The equation by which the mechanical power converted in the rotor is calculated is as follows:

$$P_{\text{Mechanic}} = 3I_2^2 \cdot \frac{R'_2(1-s)}{s} \tag{2.10}$$

where the term I_2 refers to the current that pass thorough the resistance.

Thanks to this equation, it can be seen how this mechanical power is determined by the slip of the machine, resulting in the fact that at lower slip, greater power is produced, while if, on the contrary, the slip increases, the power will be reduced due to factors such as heat losses.

Power Losses

To understand power losses in induction motors, it is necessary to look at the diagram in the Figure 2.9. It illustrates the complete power path during the normal operation of the motor. First, the total power supplied to the motor, referred to as P_1, corresponds to the active power supplied to the stator. Once this power enters in the stator, a portion of it is dissipated due to copper losses and magnetic losses. These losses are caused by the core resistance and the magnetic reactance respectively.

The resulting power output, referred to as P_2, serves as the power input to the rotor, where additional copper losses occurs, along with mechanical losses (P_m). Finally, before providing the power output, referred as P_{OUT} or BHP, the motor suffers additional losses due to friction and windage with the shaft.

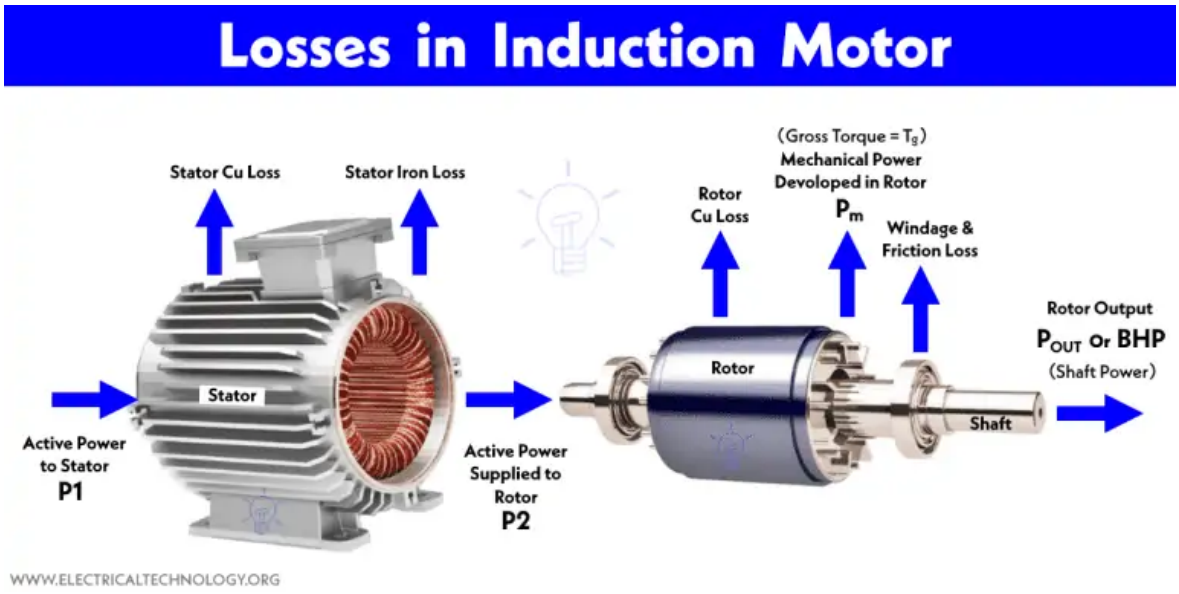

Figure 2.9: Schematic diagram of power losses on and induction motor [17]

Start-Up

Regarding the start-up of the induction motors, its necessary to discern between the two possible connections: star and delta.

Star connection is made by joining one end of each stator coil to a common point, called the neutral point. In this configuration, the phase voltage[8] is equal to the line voltage[9] divided by $\sqrt{3}$, which is approximately 57.7% of the line voltage, while the phase and line currents remain the same value.

[8] Voltage in the coil
[9] Voltage between two supplying lines

The delta[10] connection is made by joining the ends of the stator coils together to create a closed loop. Unlike the star connection, it is in this type that the phase current is approximately 57% of the line current, while the line and phase voltages have the same value. Both connections can be seen in the figures below.

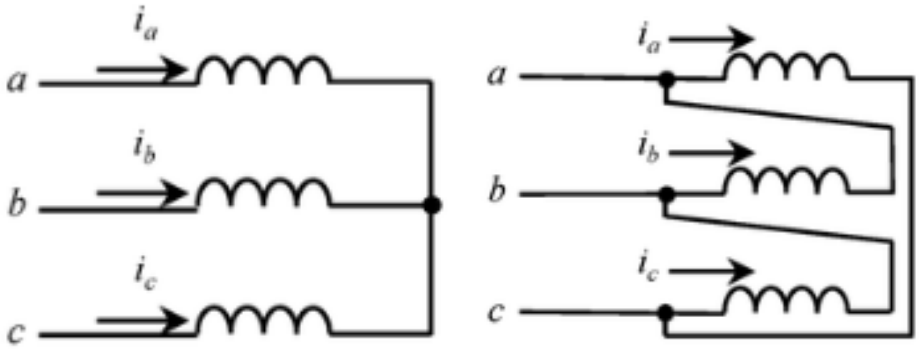

(a) (b)

Figure 2.10: Possible connections in an induction motor: 2.10(a) star and 2.10(b) delta. [18]

The initial direct outcome of these distinctions is evident in motor torque. This parameter, with the star connection, is approximately one-third of that which would be obtained with a triangle connection. This is because the torque is proportional to the square of the applied voltage, as the following equation indicates:

$$T \propto V^2 \tag{2.11}$$

On the one hand, this means that for start-ups, where the initial torque is not a primary concern, and for applications requiring a low initial load, the star connection is ideal. On the other hand, for applications requiring a higher current demand or for applications with a heavy load, the delta connection is a suitable option.

In this way, one of the most classic methods for starting induction motors is developed: the star-delta starting. During start-up, the stator is star-connected, which implies a reduction in its voltage, a reduction in current demand and consequently a lower torque. Once the machine has reached steady state, this connection of the stator coils is automatically switched to delta, where it will remain for the rest of the time. This change occurs when the motor operators deem it appropriate [19].

[10]The terms triangle and delta are synonymous and will be used interchangeably in this text.

Thanks to this method, the thermal stress on the motor produced during start-up is reduced and good efficiency is maintained in the steady state. This method requires switching time between the different connections, which does not make it feasible for all applications, due to the voltage drops and current peaks produced during this period.

Chapter 3

MODELLING SETUP

This chapter discusses the modelling of a high voltage IM and the description of the study case system. The simulation model is created using advanced modelling techniques and software such as AutoCAD and SIEMCENTER MAGNET.

The motor under study is a squirrel cage IM, which is widely used in industrial applications. This type of motor is simple and can maintain a constant speed regardless of the load it is carrying.

3.1 Model Description

In this section, the characteristics of the induction motor and the process used to build the model are detailed below in table 3.1. These characteristics will be important in order to simulate the model with the greatest possible accuracy, so it is necessary to compare them with the values obtained on the set-up simulations, which are detailed in Table 3.2.

Parameters	Delta value	Star value
Voltage	400 V	690 V
Power	4 kW	4 kW
Current	8.5 A	4.9 A
Pole pairs	4	4
Stator slots	48	48
Rotor slots	28	28
Nominal Speed	1455 min-1	1455 min-1

Table 3.1: Characteristics of the IM under study

Parameters	Delta Measurements	Error (Delta)	Star Measurements	Error (Star)
Power	4.4 kW	6.2439%	4.4 kW	6.92%
Current	8.9681 A	5.28%	5.2232 A	6.38%
Nominal Speed	1471.2 min-1	1.09%	1470.8 min-1	1.11%

Table 3.2: Steady characteristics of the healthy IM simulations under delta and star connection

As it can be seen, the errors obtained in the models produced are less than 10%. Taking into consideration the approximations and assumptions made in the modelling, this error indicates a close resemblance to the theoretical model to be studied.

3.2 AutoCAD Design

The first step of the IM modelling process is necessarily to create a schematic design. The geometry of this design, shown in the Figure 3.1 below, has been created by AutoCAD software, which allows the different components of the model to be created.

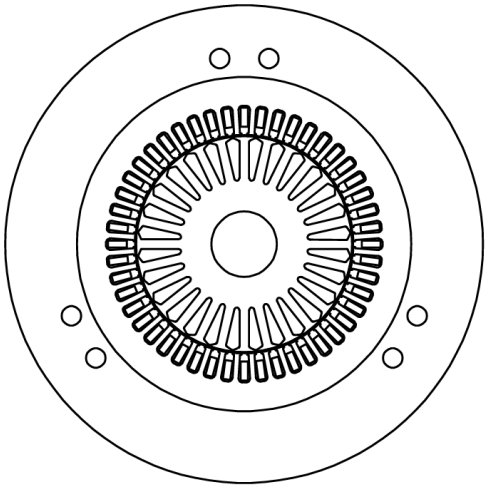

Figure 3.1: 2D outline of the IM made on AutoCAD

For the motion component of the motor, it has been necessary to add an air gap of four layers, which can be seen in Figure 3.2. This space has been made only with one layer of 1.5 mm of distance, to ensure precision on the electromagnetic simulation to prevent the collisions that might be produced during the motor's normal operation and make the simulation unable to run. The measurements for all the components of the design were given to simulate a real IM.

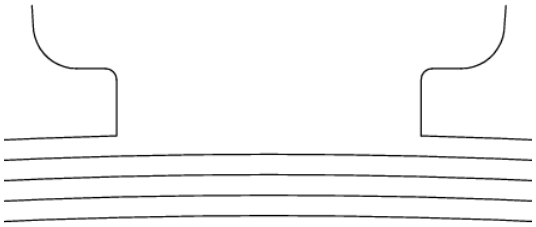

Figure 3.2: Design of the 4 layer air gap made on AutoCAD

Also, to be the most accurate possible to the real IM model, it has been made an air box around the motor to ensure its work on a correct space. This element is viewable in Figure 3.1 as an outer circumference, which is elaborated by means of virtual air.

In the next step, this design will be imported into SIEMCENTER MAGNET software to continue with the modelling setup.

3.3 Magnet Design

After the design of the IM on AutoCAD, the final step is the creation of the different components, resulting in the model seen in Figure 3.3. This creation will be made on SIEMCENTER MAGNET software, which allows the user to change the parameters of the model, such as the active length of the machine, the properties of the materials used in each component, and how the coils are connected between them.

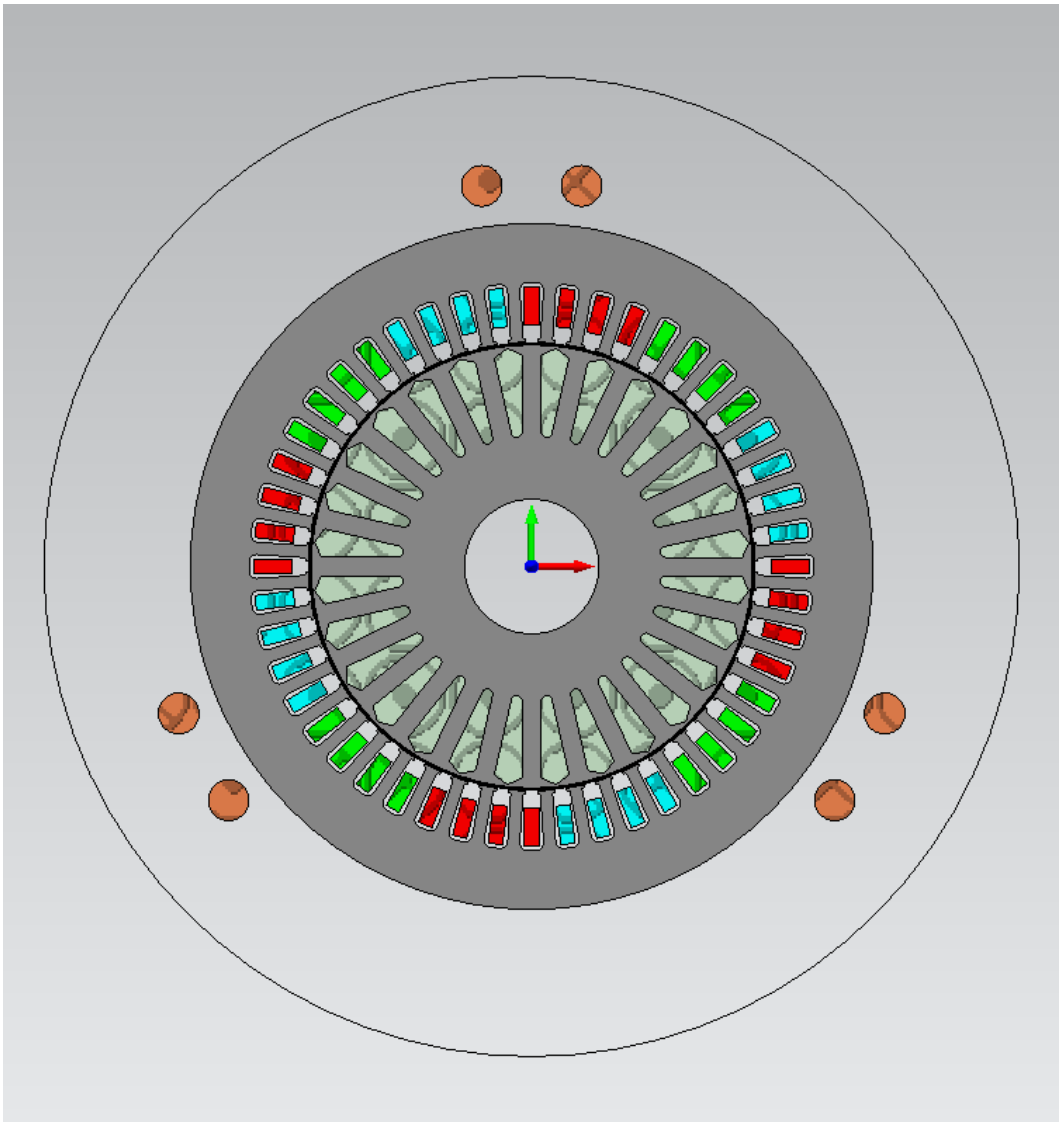

Figure 3.3: Final model of the IM made on Magnet

Stator

To make the stator, it is required to make a new magnetic material to achieve the specifications required on the model. This material is shown in Figure 3.4 and its properties are based on the material "AISI 1010 Steel, cold drawn", which is provided by the magnet software. The parameters of the density and the magnetic permeability were changed to improve the model's accuracy.

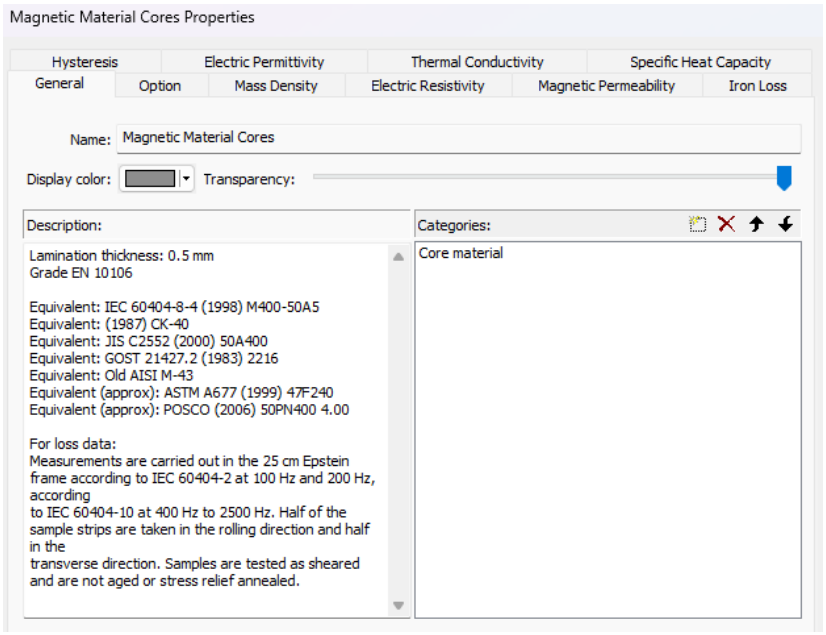

Figure 3.4: Properties of the magnetic material used for the stator and rotor cores.

This stator was made with 48 slots, meaning the motor will have 16 slots per phase and 4 slots per pole. Having more than one slot per pole provides a lot of benefits to the motors' normal working, like a a more uniform distribution of magnetic flux, less harmonics on the electromagnetic force or an easiest way to design the connections of the coils.

Rotor

As the stator, the rotor core was made with the same magnetic material, shown in Figure 3.4. In this case, the rotor only includes 28 slots, the rotor bars, inside his core. These bars are made of aluminium, and their description and categories are shown in Figure 3.5. The choice of creating the bars with this material has been made by the electrical and thermic properties of it and its low price. Also, aluminium is a lightweight material that allows the easiest fabrication and a decrease in the weight of the entire model. These rotor bars have

been turned into solid coils to create the end rings[1] of the IM. These end rings allow electrical fields' current to pass trough while the rotor is moving.

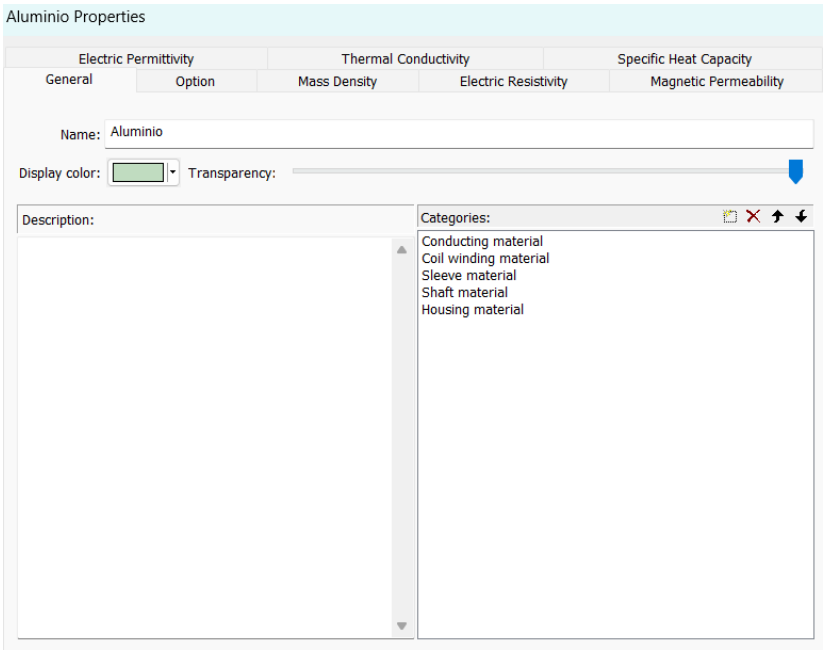

Figure 3.5: Properties of the aluminium material used for the rotor bars.

Air Gaps

As has been said, to prevent collisions, there is an air gap of 4 layers, the stator air, the stator VA, the rotor air, and the rotor VA. These layers were created in two different materials, air, and virtual air, which are shown in Figure 3.6 and Figure 3.7 respectively. These materials allow the software to simulate the movement in real conditions.

In the case of virtual air, it creates a frictionless zone around the component, allowing the simulation to run. This is a requirement for the software, since if the component is surrounded solely by air, it would generate friction that would prevent it from moving. It is also necessary because if a strip of air is included in the moving element, the software would detect a non-fluid material and abort the simulation.

[1]The ring at either end of an induction motor rotor to which the copper or aluminium bars are connected

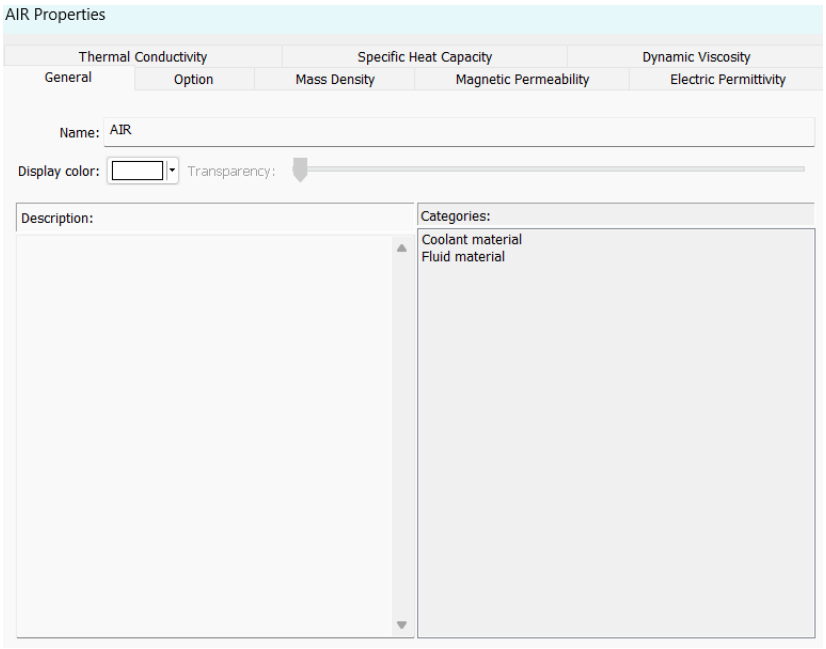

Figure 3.6: Properties of the air material used for the air gaps layers and the air box around the model.

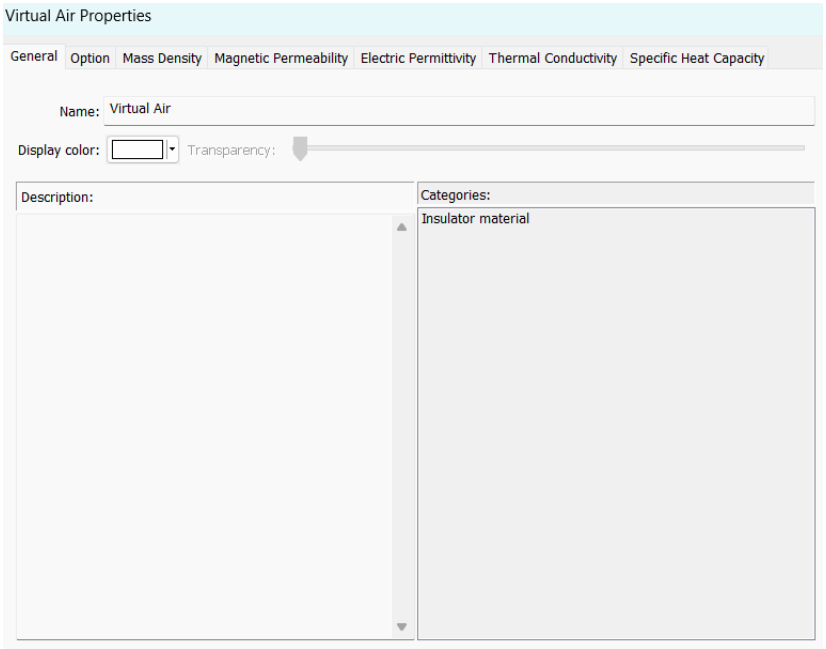

Figure 3.7: Properties of the virtual air material used for the air gaps layers.

Coils

For the coils, there are three different phases on the motor. To make them, there has been defined three materials with the same properties as the copper provided by the software,"Copper: 100 IACS", but with the only difference of changing the colours to make it easier distinguish the phase of the coil. In each phase, the motor has 8 coils, with 40 turns each, that were created separately.

For the first phase, or phase R, the coils were named $Coil - R_{1X}$ for the input and $Coil - R_{2X}$ for the output, where they going to $Coil - R_{18}$ and $Coil - R_{28}$. The material used for this phase is shown in Figure 3.8.

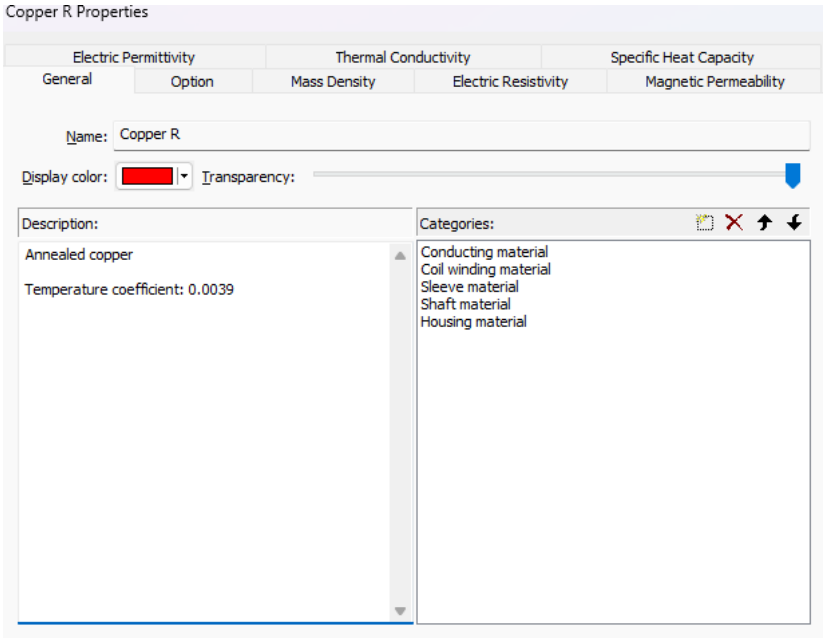

Figure 3.8: Properties of the copper material used for the coils of phase R

For the second phase, or phase S, the coils were named $Coil - S_{1X}$ for the input and $Coil - S_{2X}$ for the output, where they going to $Coil - S_{18}$ and $Coil - S_{28}$.The material used for this phase is shown in Figure 3.9.

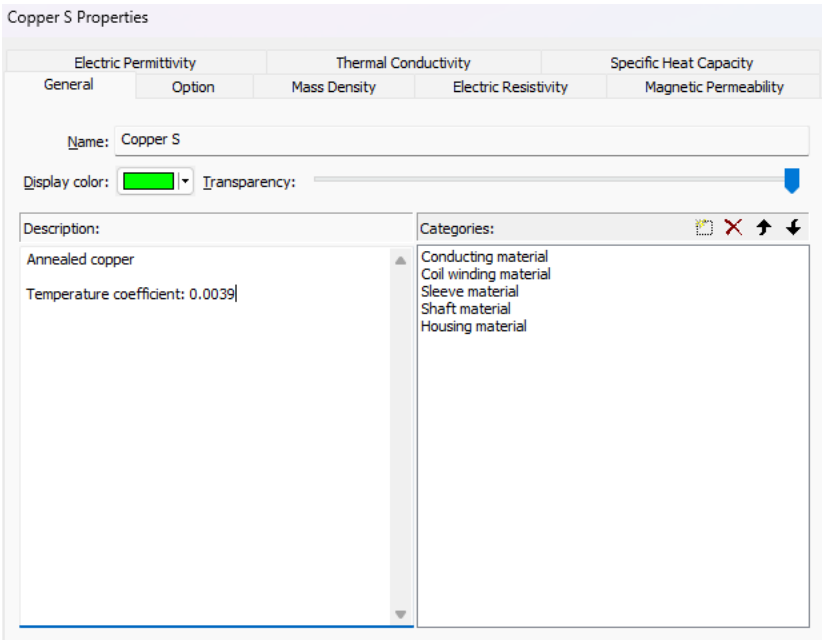

Figure 3.9: Properties of the copper material used for the coils of phase S.

For the third phase, or phase T, the coils were named $Coil - T_{1X}$ for the input and $Coil - T_{2X}$ for the output, where they going to $Coil - T_{18}$ and $Coil - T_{28}$.The material used for this phase is shown in Figure 3.10.

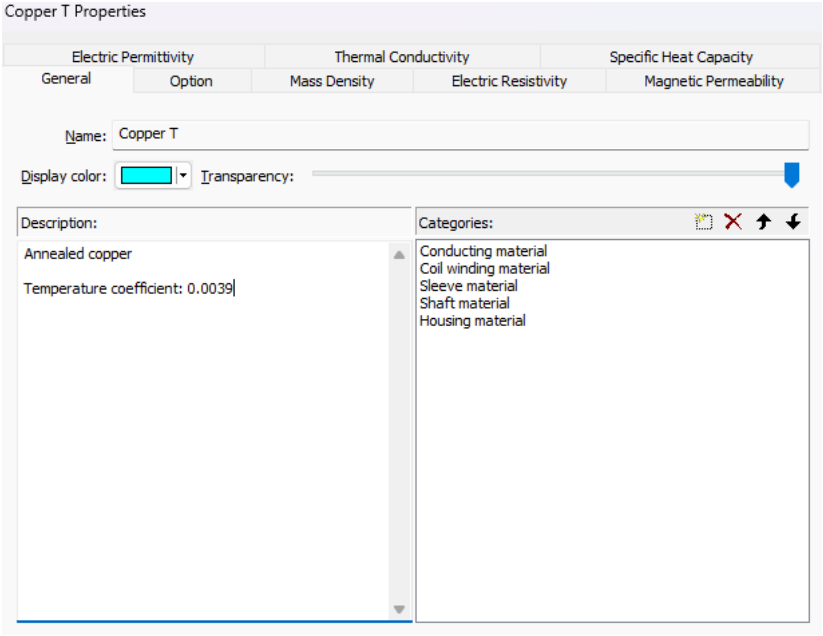

Figure 3.10: Properties of the copper material used for the coils of phase T

To be as accurate as possible to the real model, the input and the output of the coils were connected following a subtype of concentric pattern. The main concentric pattern can be observed in Figure 3.11. For this case and to achieve the most uniform magnetic field possible, the order of the connections has been changed, where now the first coil of the pole is connected to the first coil of the next pole and so on. With this type of pattern the magnetic field produced is as sinusoidal as possible, making it more strict.

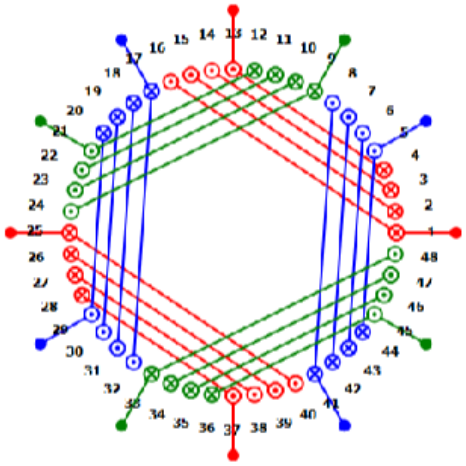

Figure 3.11: Concentric pattern used to match the input and output of the coils on the IM.

Sensors

To manage how the magnetic field changes along the simulation, there has been disposed three sensors around the stator core of the motor. These sensors are made by designing a coil composed by two copper cylinders of 8 mm of diameter and 150 mm of length as is shown in Figure 3.12(a). This cylinders were named Sensor 1 and Sensor 2 for the input and output of the coil respectively. These sensors have also been positioned close enough to the stator to pick up the magnetic field measurements but far enough away so as not to disturb them.

This sensors are connected to resistances with a high value, 10 TΩ in order to make the flux current along them the less value possible. With this change, shown on Figure 3.12(b) it is possible to convert them in an ideal voltage sensors, allowing them to measure with more accuracy. This type of sensor relate the voltage measured with the time derivate of the magnetic flux on a direct way, like is shown on the equation 2.5 explained on the Chapter 2.

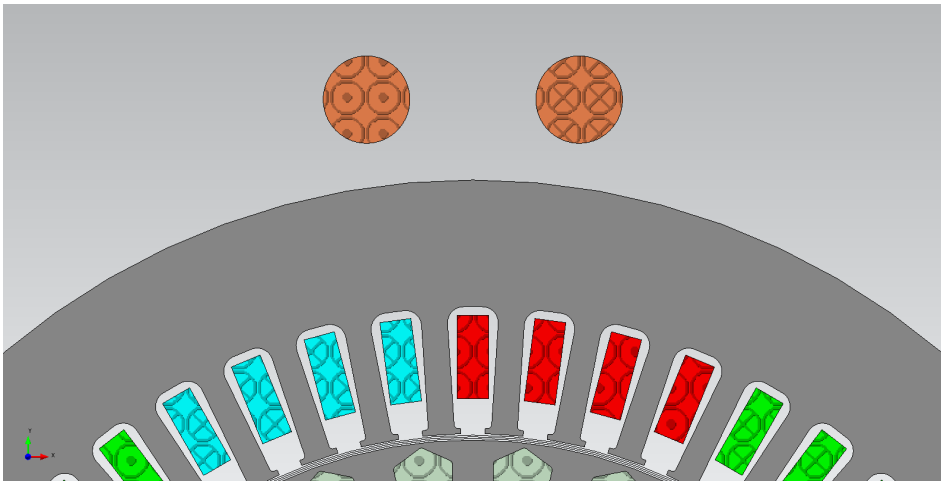

(a)

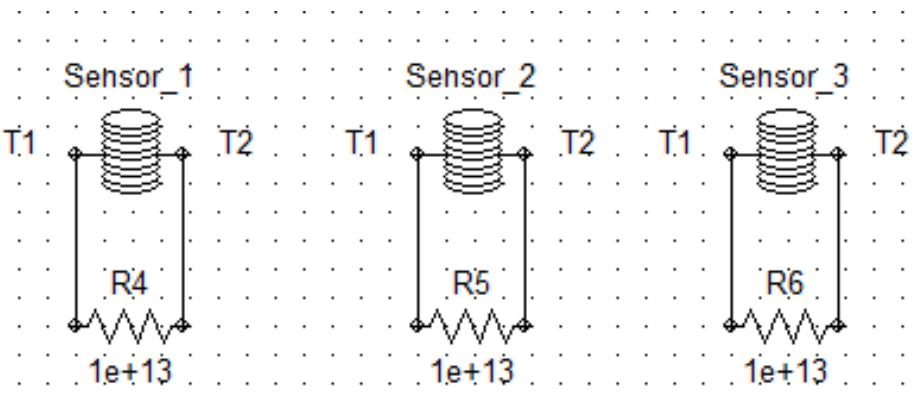

(b)

Figure 3.12: Sensors placed around the IM model: 3.12(a) modelling of sensors and 3.12(b) connection of the sensors

Circuit

For the creation of the IM model circuit, the coils of the same phase have been connected in series with their respective resistor. This circuit, in order to be able to compare results, has been made in both star and delta connections. For the delta connection, the first coil of each phase has been connected to the last coil of the previous phase, creating a triangle with the three phases. On the other hand, the star connection is made by connecting the coils around a common neutral. The differences in these connections will be used for further analysis.

The Figure 3.13 and the Figure 3.14, which are shown below, illustrate how the delta and star connection are made on the modelling.

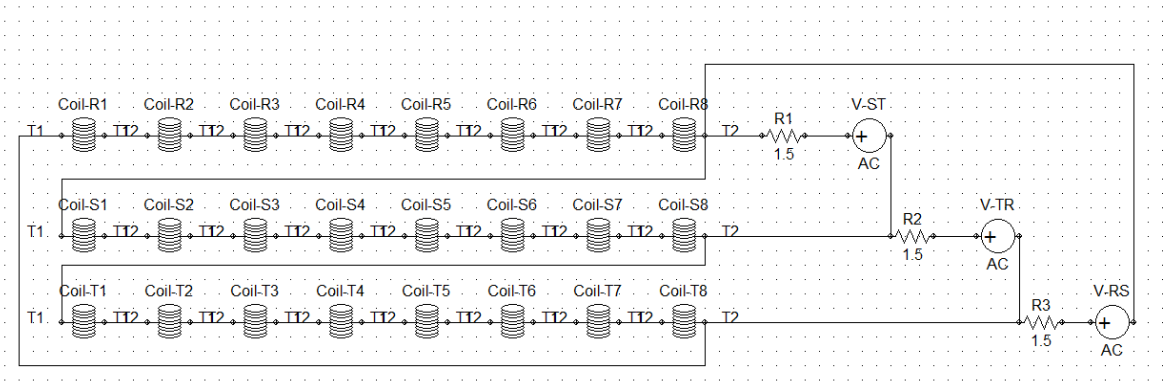

Figure 3.13: Elaborated circuit of the IM model in the delta connection

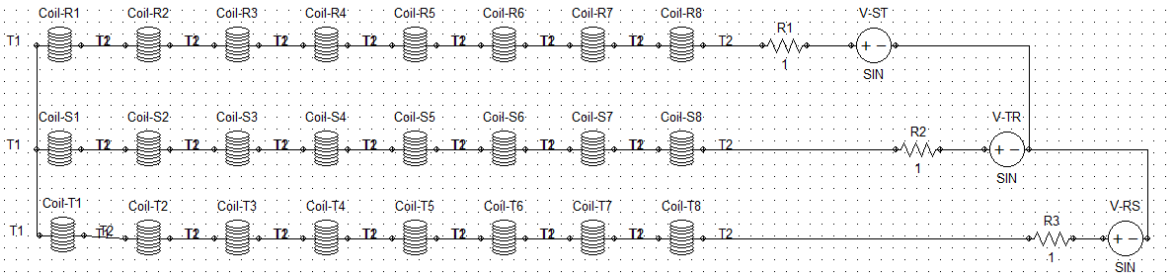

Figure 3.14: Elaborated circuit of the IM model in the star connection

As it can be seen in the previous Figures, three resistors have been added to the phases. These components represent the resistance value of the coils on the phase, and they must be calibrated to the best value to ensure the accuracy of the model.

It is also possible to see how the three voltage sources are placed in the circuit. These sources have been modified to meet the requirements of the motor by changing their amplitude and phase values. In the case of amplitude, despite the connection used, the way to achieve the desired value is given by the equations 3.1 and 3.2 below.

$$V_{RS} = \frac{V_{RN}}{\sqrt{3}} \tag{3.1}$$

$$V_{RN}(Peak) = V_{RN}(RMS) * \sqrt{2} \tag{3.2}$$

The three of the voltage sources has been offset by 120° from each other. This offsetting needs to be to make the rotor move in the correct direction.

To facilitate the model, it has been chosen to use the AC voltage sources with the voltage magnitude (RMS) required in each connection.

As a final step, to create the rotor circuit and the end rings, it has been decided not to place their resistance on the circuit. This choice has been made because, in this model, the motion component is load-driven, which means that its speed will oscillate over time, making the slip variable. This slip, as is shown in Equation 2.9, is critical to calculating the resistances of the end rings, as it can be shown in Equation 3.3 [20], [21]. Due to this, for the simulations of this thesis, it is supposed that these elements have no resistance, because the difference of it if they have it or not is not relevant for the results, being the values generated valid and acceptable for the correct development of the thesis.

$$R_r(s) = \frac{R_b}{s} \tag{3.3}$$

where $R_r(s)$ is the resistance of the , R_b is the resistance of the, s is the split of the motor.

Due to this, the circuit of the rotor has been designed like on Figure 3.15, where all of the rotor coils are connected in series.

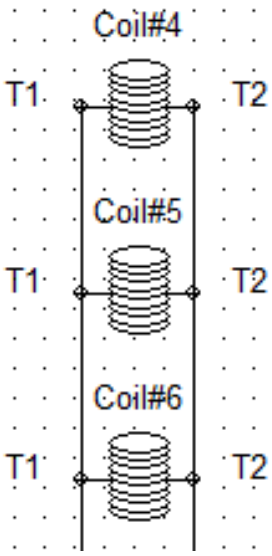

Figure 3.15: Elaborated end rings and rotors' bars circuit in the IM model

Chapter 4

STUDY CASES AND SIMULATIONS

This chapter will discuss the different simulations performed on the IM model and elaborate on the analysis with the obtained results. These analyses will mainly consist of comparing the healthy IM model with the ones made with a typical fault on the induction motors: the rotor broken bars. The simulations will be executed with the two types of connections, star, and delta, with the final goal of make a comparative analysis of the impact of these faults on model under investigation.

4.1 Fault Condition Applied

The broken rotor bars are the most common fault in induction motors. Factors like excessive mechanical stress, overheating, or manufacturing defects can cause these types of faults. As a result, the rotor operates asymmetrically, leading to numerous problems within its normal work, like undesired vibrations, an increase in the noise, unbalanced currents, decrements in the motor efficiency, and in several cases, the breakdown of it [22]. These problems make diagnosing the broken bars a crucial step in motor development. Once identified, repairing or replacing the affected rotor or motor is mandatory to restore optimal performance and reliability.

4.2 Condition Monitoring Techniques

MCSA

Motor current signature analysis (MCSA) is a system used to analyse dynamic energized systems. The result that it provide assist the operator to detect: incoming winding health, rotor and stator health, the dynamic eccentricity in the air-gap, load issues and many other crucial parameters for the correct performance of the systems [23]. This system is therefore established as a one of the most powerful methods of online motor diagnosis for detecting motor faults, allowing the health of electrical machines to be analysed by means of a detailed analysis of the currents circulating in the stator. This method therefore helps with the fault's detection, with the objective of reduce the down time and the costly repairs in the electrical machines [24]

In order to carry out this analysis, some fundamental steps have to be followed to help the correct development of the analysis. These steps are described as follows:

1. Perform an overview of the system to be analysed.
2. Determine what kind of faults are to be analysed in order to find out why the machine is malfunctioning.
3. Obtaining the stator current. In this step, data is processed in order to make it more accurate and reliable for the following steps.
4. Data review and analysis. In this step, a frequency spectrogram is made in order to observe in detail the amplitude of the harmonics around the operating frequency of the machine. This frequency spectrum is performed by FFT.

In the field of induction motors, this technique focuses on the analysis of the sidebands generated in the surroundings of the operating frequency. Due to the anomalies of the rotor when bar breaks occur, a backward RMF is produced in the slip frequency with respect to the normal forward RMF. The backward RMF at slip frequency induces an electromotive force, and a current in the stator winding at:

$$f_{sb} = f_1(1 - 2\ s)\text{Hz} \tag{4.1}$$

This sideband, as shown in the equation, is generated to the left of the operating frequency and owes its origin to rotor bar breakage. This is not the only sideband that is produced and that can be observed in the spectrogram, in a 'symmetrical' way a right sideband is also produced, which owes its origin to the speed oscillation that is produced in the rotor. This speed oscillation can affect and reduce the amplitude of the left sideband. Rotor bar breakage therefore results in induced current components in the rotor winding at frequencies:

$$f_{sb} = \text{fl}(1 \pm 2\ s)\text{Hz} \tag{4.2}$$

The MCSA has many advantages including no motor parameter estimation and the simplicity of the current sensors and their installation. It provides a highly sensitive, selective, and cost-effective means for online monitoring of a wide variety of heavy industrial machinery. But as powerful as this technique is, it is not omniscient. There are certain types of failures that can elude the clutches of this method. Some mechanical faults, which occur in unlikely patterns, may not show up prominently in the current spectrogram, resulting in them passing as healthy results [25].

Not only certain types of faults can alter the results of the analysis, but also external factors such as ambient conditions, electrical noise or load variations can affect the accuracy of the

results. This means that the calibration of sensors, proper installation, and the quality of data acquisition devices play crucial roles.

Understanding these shortcomings, it is understood that this method is not the panacea for all types of issues that can afflict electrical machines, needing to be used in conjunction with other technologies, such as motor circuit analysis, in order to provide a complete overview of the motor circuit

SFSA

The stray flux signature analysis, or SFSA, is a method of signal analysis based on the study of the measurement of magnetic flux 'leakage' from an electrical machine, such as an induction motor. This lost flux contains the necessary and important information to know the internal state of the machine and to check if it presents anomalies in its operation. For this analysis, it is necessary to differentiate between two types of flux leakage depending of their direction: radial and axial. Radial leakages escapes outside de yoke[1], while the axial leakages escapes through the rotor shaft.

In order to measure these leaks, a number of sensors have to be placed around the engine. If only axial leakage is to be analysed, these sensors must be placed along the axial surface, enclosing the shaft. If, on the other hand, both axial and radial leakage are to be analysed, the sensors must be placed along the radial surface of the motor frame. As explained earlier in the modelling chapter, these sensors are made up of coils with a large number of turns and connected to high value resistors, in order to make them sufficiently similar to ideal voltmeters. An example of this leakages can be shown in the figure 4.1 below.

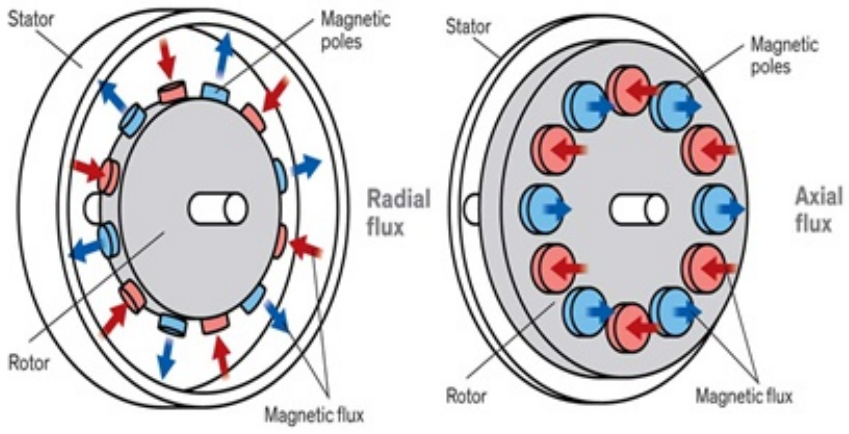

Figure 4.1: Representative diagram of radial and axial flux leakage in an induction motor.

[1]The outer part of the stator core that holds the stator mechanically and completes its magnetic circuit.

This technique is non-intrusive and it is not necessary to dismantle the motor to perform it. It also has the advantage of providing early diagnosis of electrical and mechanical faults as a complementary aid to other techniques such as vibration analysis or stator current analysis (MCSA).

4.3 Magnetic Flux Density

The FEA model provided by the SIMCENTER Magnet software allows the magnetic flux density of the model to be observed over several instants, as shown in the following figures. In a healthy instance and under nominal performance conditions (Figure 4.2), it can be observed how the flux lines are uniformly distributed in both the rotor and the stator, creating four poles in the magnetic field and exhibiting a symmetrical and uniform pattern. This flux distribution serves as an indication of a balanced performance, where each pole contributes equally to the electromagnetic torque production.

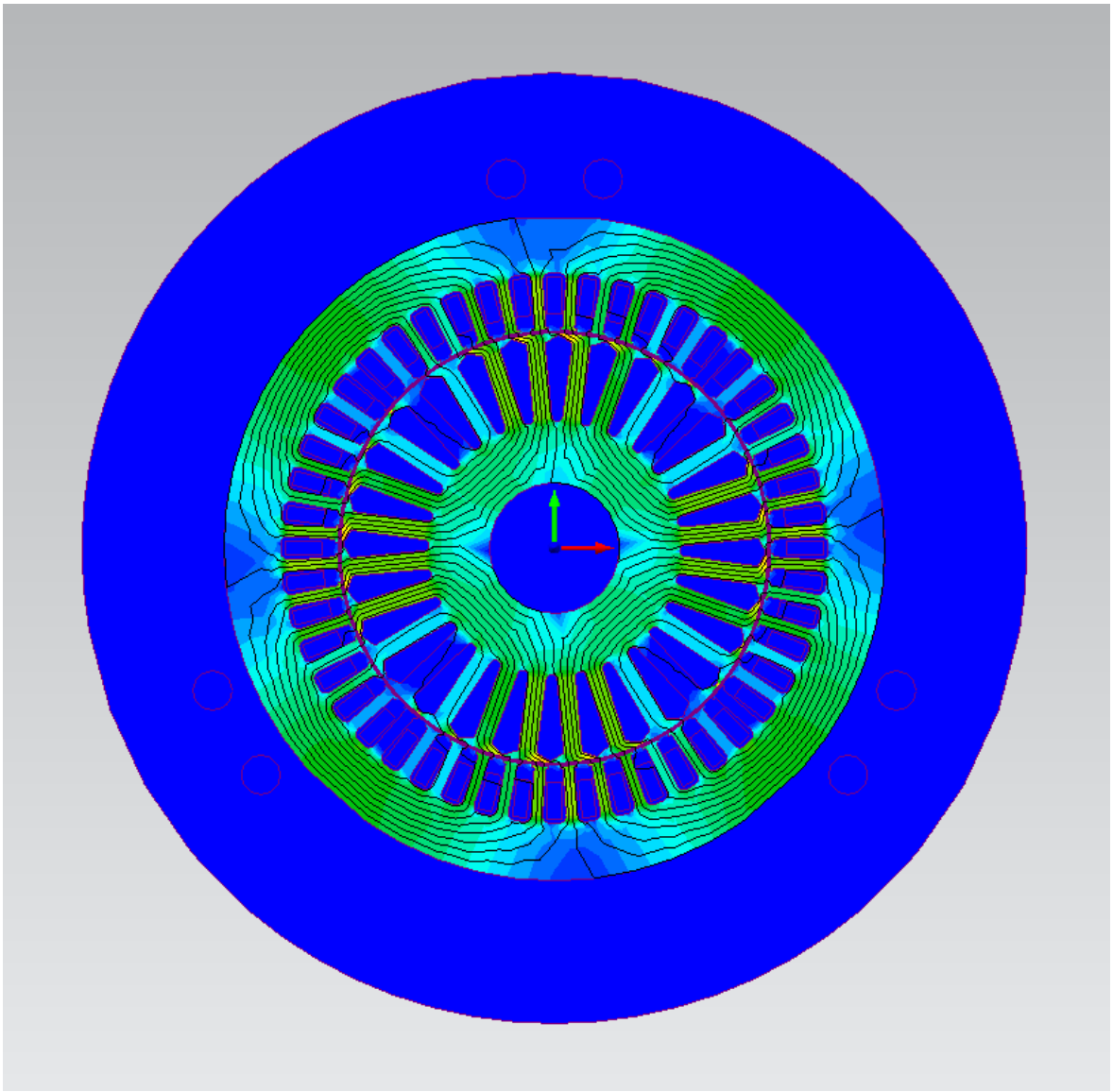

Figure 4.2: Spatial distribution of the magnetic flux while at steady state under nominal and healthy operation in star connection at 30 milliseconds

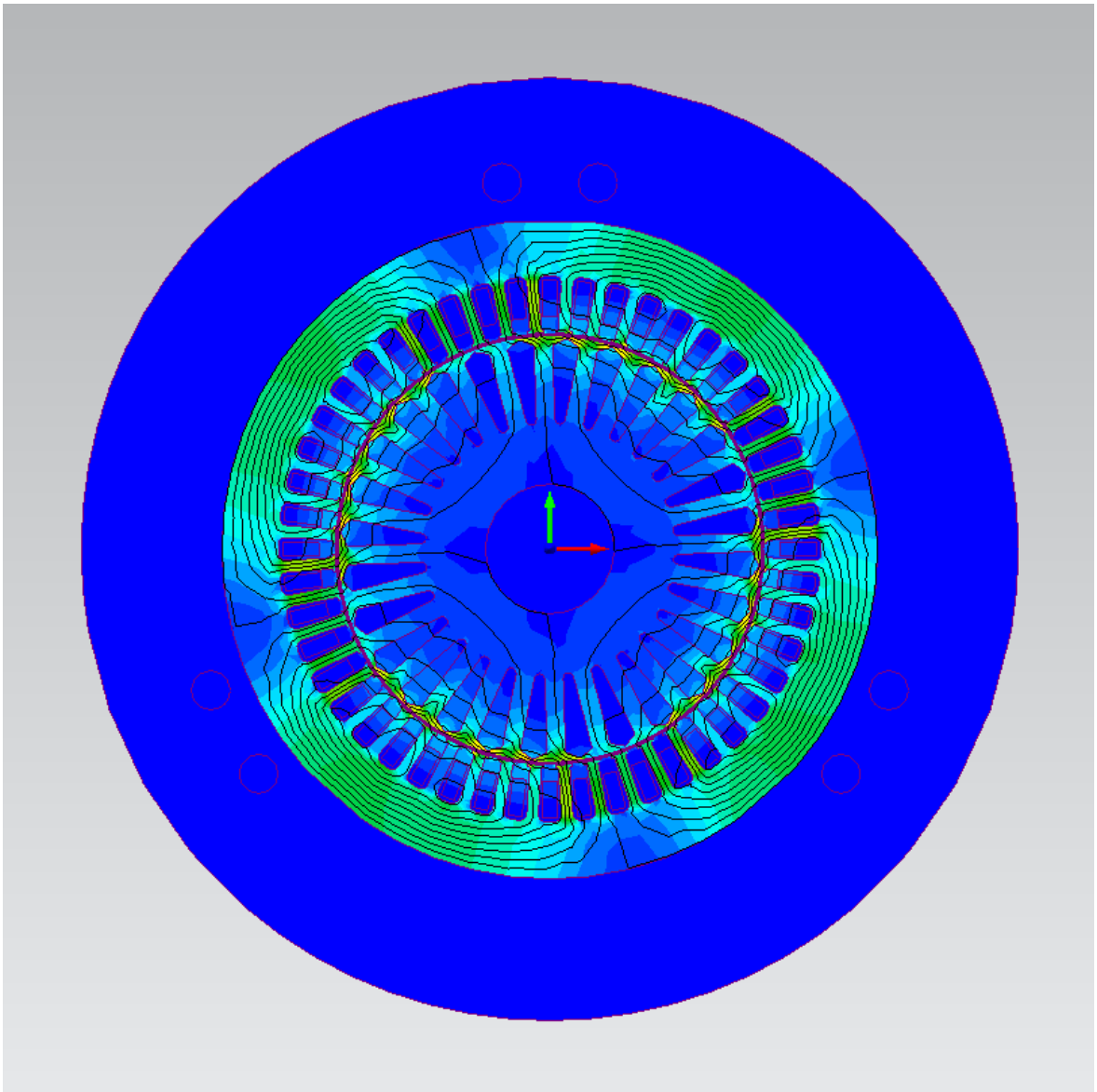

Figure 4.3: Spatial distribution of the magnetic flux while at steady state under nominal and healthy operation in star connection at 3000 milliseconds

These figures facilitate the observation and understanding of the phenomenon known as the skin effect. During the start-up phase, as shown in Figure 4.3, the magnetic field tends to concentrate on the rotor's surface. The phenomenon of the skin effect appears when a RMF penetrates the melt with electrical conductivity, due to the alternating currents induced in the rotor [26]. In the IM, this effect is caused by the currents induced by the RMF of the stator. This field not only induces the currents that make the rotor rotate following the movement of the field but also induces certain parasitic currents in the rotor, which, according to Lenz's law outlined in Chapter 2, tend to oppose this variation. The presence of these parasitic

currents leads to the concentration of the inducted currents on the surface of the rotor, instead of being distributed uniformly throughout its volume. This effect occurs during the start-up phase because it is in this state that the motor demands a large amount of current in order to overcome the initial inertia and rotation. This non-uniform distribution of the field results in additional heating in the motor, which affects its performance and efficiency, making this effect crucial when designing IMs.

Rotor Bars

The results obtained from the FEA model about the flux distribution of the magnetic field demostrate the impact of the faults in it, as illustrated in the following Figure 4.4.

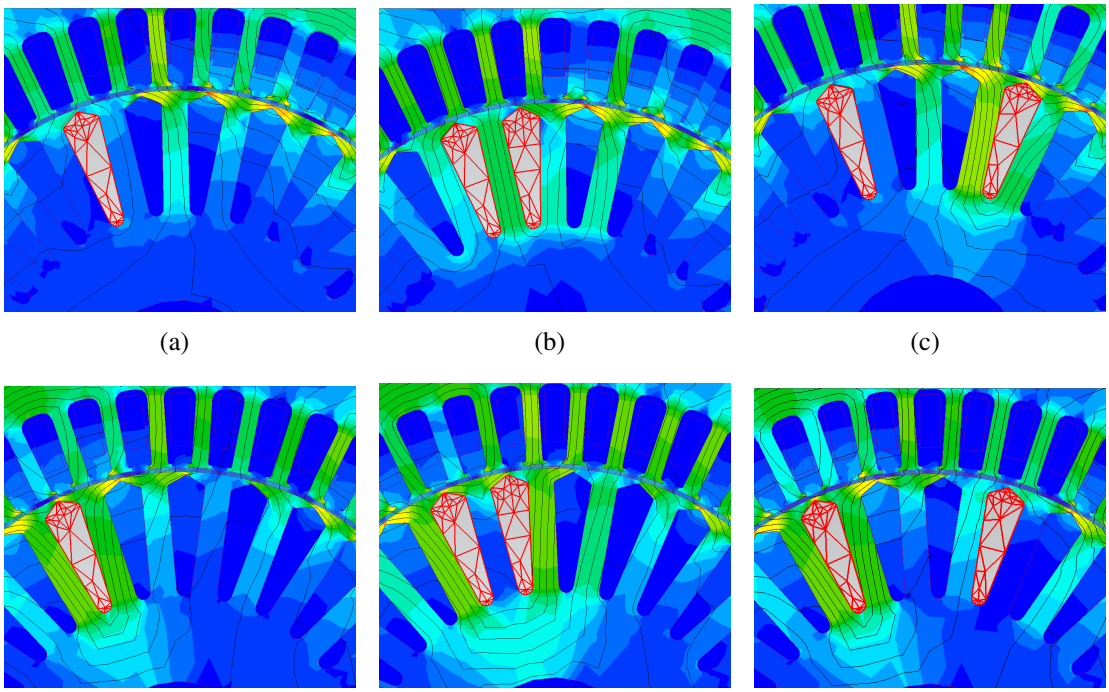

Figure 4.4: Magnetic flux spatial distribution near the broken bars: 4.4(a) 1 broken bar in delta connection, 4.4(b) 2 adjacent broken bars in delta connection, 4.4(c) 2 non-adjacent broken bar in delta connection, 4.4(d) 1 broken bars in star connection, 4.4(e) 2 adjacent broken bars in star connection and 4.4(f) 2 non-adjacent broken bars in star connection.

As it can be seen, the breakage of the bars produces a considerable increase in the magnetic field flux in the surroundings of the damaged bars. These anomalies can be noticed most clearly in the starting phase of the motor, because it is during this state, as explained above, that the motor demands more current compared to the steady state.

4.4 Stator Current Analysis

In the study of this thesis, the first step involves a comprehensive analysis of the stator current for all previously described simulations. This analysis covers both the steady-state and transient starting phases of the motor, providing insight into the behaviour of the motor under healthy and fault conditions.

Current Density

In order to observe how the faults caused in the model affect the current density and be able to identify those faults, is necessary to plot a circular contour graphic, where this current density will be visible at each rotor bar along the perimeter of the rotor.

As it can be seen in the following figures 4.5 and 4.6, each on a different connection, when a bar of the rotor breaks, the current density of the other bars is altered.

In the case of the Figure 4.5, it can be seen that when a bar breaks, it suffers a considerable decrease in current, while the bars closest to it suffer an increase in current. This growth effect in the adjacent rotor bars is due to the motor's need to compensate for the loss of current produced by the breakage, in order to be able to overcome the initial inertia and rotation of the motor. The broken rotor bars are marked with arrows to facilitate their visualisation.

The same behaviour can be seen in Figure 4.6, which shows the current density of the rotor bars in the model developed with the star connection. Although in most cases the behaviour is broadly the same, an anomaly arises when dealing with two adjacent rotor bars. In this case, when the second bar breaks, it does not cause a decrease in its own current density, but forces the two bars closest to the left to equalise, and it is they who suffer from the current reduction. This does not prevent the characteristic increase in current in the third nearest rotor bar from being observed.

This effect in the star connection is due to the lower current demand at motor start-up compared to the delta connection. This change means that as less current is required, the magnetic field generated in the rotor is less intense and more diffuse, making the magnetic field distribution more homogeneous.

These results provide a more objective point of view on this type of analysis, suggesting that although the resulting data are acceptable in certain cases of operation, they are not sufficiently reliable to depend solely on them as a preventive method. As it can be seen in the figures, this method corresponds to a dynamic method that studies the values at a given moment, which means that the global behaviour of the engine is not studied and can give rise to false results.

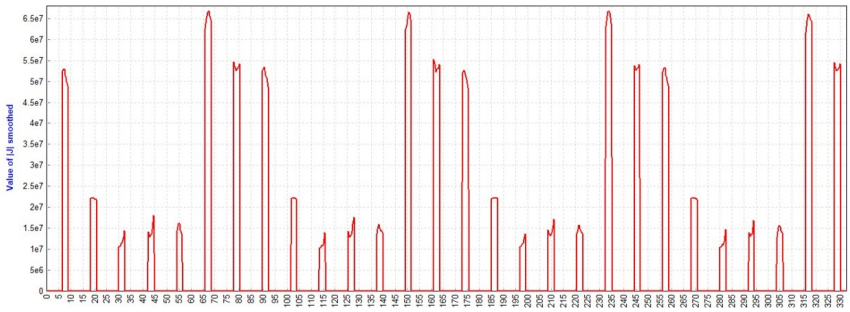

(a)

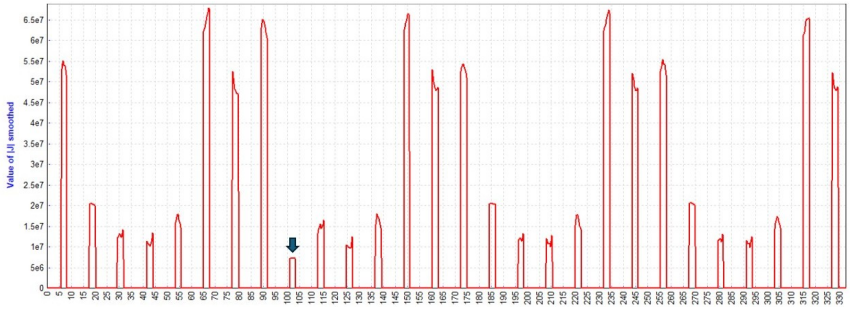

(b)

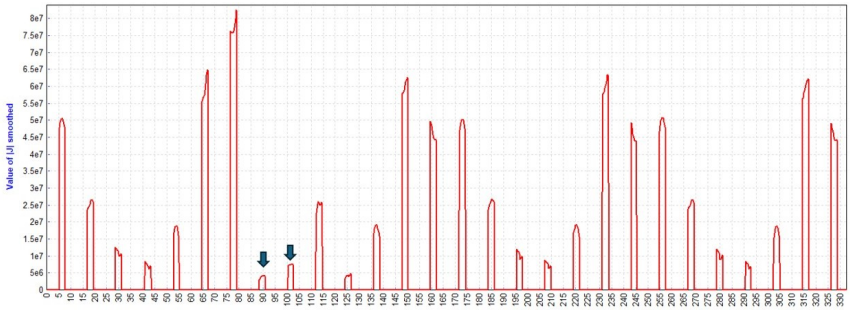

(c)

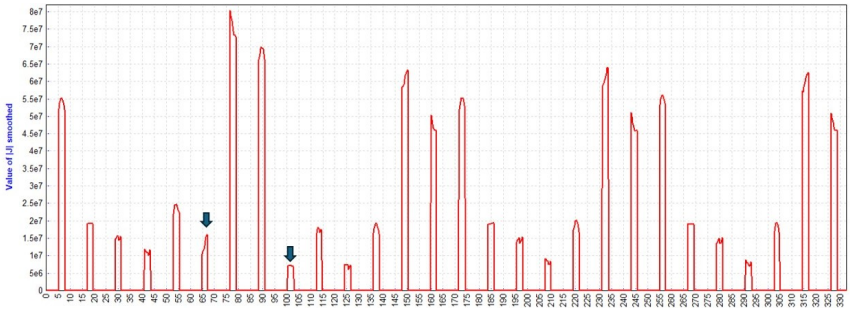

(d)

Figure 4.5: Current density absolute values on motor's rotor bars with delta connection: 4.5(a) Healthy, 4.5(b) 1 broken bar, 4.5(c) 2 adjacent broken bars and 4.5(d) 2 non-adjacent broken bars

.

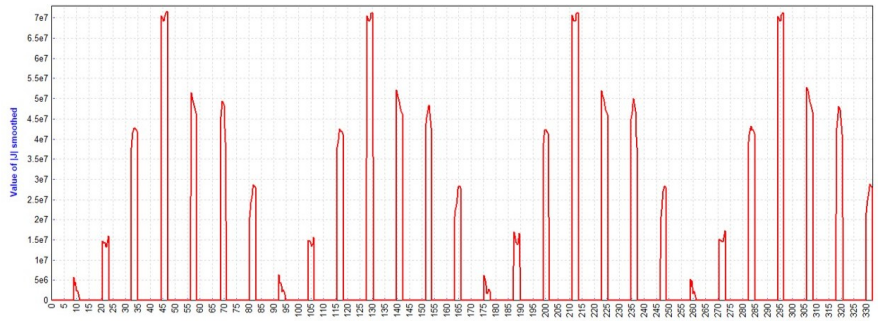

(a)

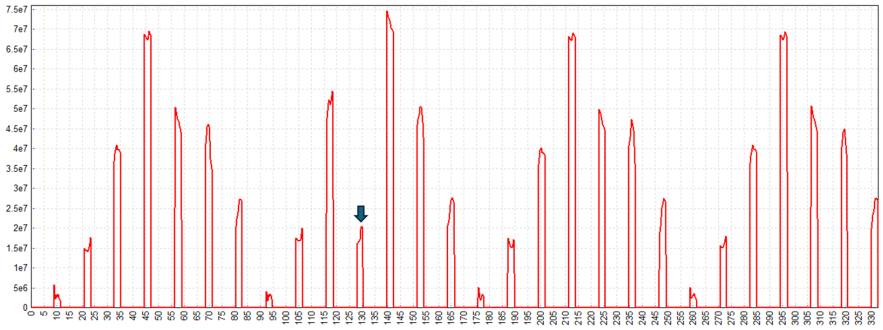

(b)

(c)

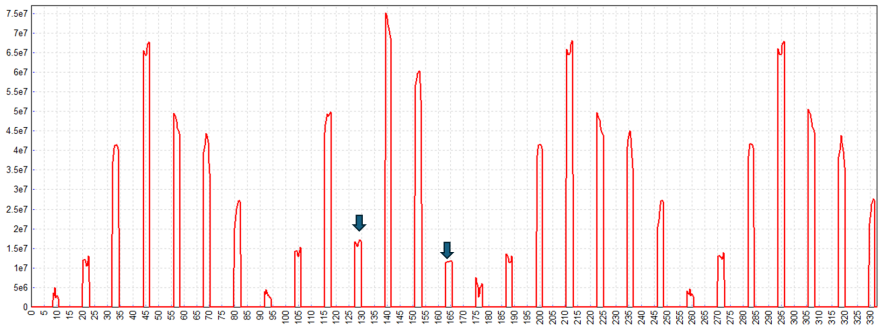

(d)

Figure 4.6: Current density absolute values on motor's rotor bars with star connection: 4.6(a) Healthy, 4.6(b) 1 broken bar, 4.6(c) 2 adjacent broken bars and 4.6(d) 2 non-adjacent broken bars

.

Time Domain Current

This analysis focuses on studying the stators' electrical current state over time. In order to make this, some measurements have been made on the voltage sources located on the circuit, giving as a result the graphics seen in figures 4.7 and 4.8, where is possible to see a comparison of the current between the different study cases in the whole time of the simulation and a zoomed graphic where the anomalies of the transient state can be seen.

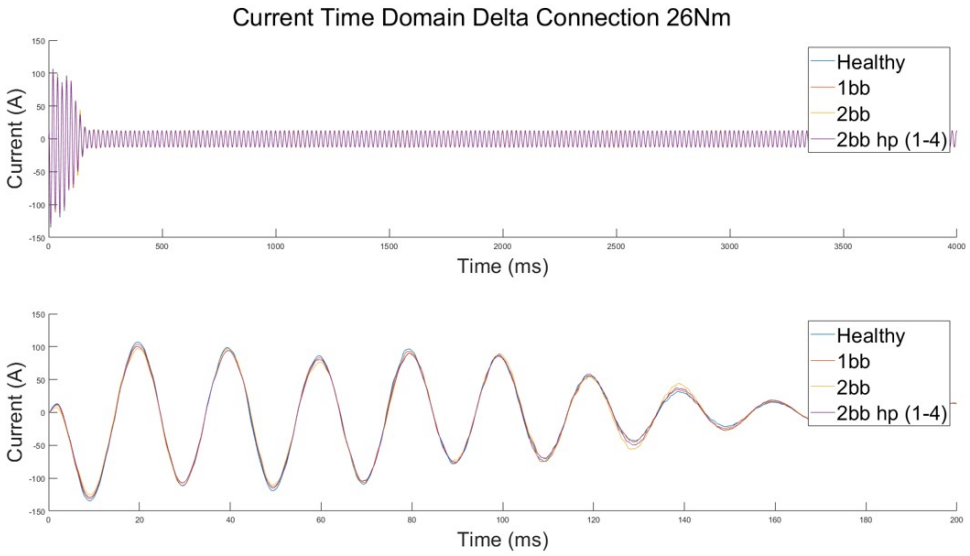

Figure 4.7: Delta current time domain in the different proposed cases: healthy, 1 broken bar, 2 adjacent broken bars and 2 non-adjacent broken bars (1-4)

Looking at the graphs, some anomalies can be observed during the transient part. In this state, the maximum peak current is reduced as a function of the number of broken bars present in the motor. The difference between the healthy model and the model with two non-adjacent broken bars is not that big, but it is noticeable enough to understand that even if the motor tries to compensate for the lack of current due to losses, it will not be fully compensated. These differences become less noticeable as the steady state is reached, where they are barely visible.

This analysis has been made in both connections, star, and delta, in order to make a comparison of the mainly differences between them. As it can be seen in Figure 4.8, while the transient state of the motor is taking place, the star connection exhibits a reduced current demand compared to the delta connection. This means that during start-ups, less torque is needed to

generate rotor spin, making the star connection the most suitable for this state and resulting in a bigger useful life.

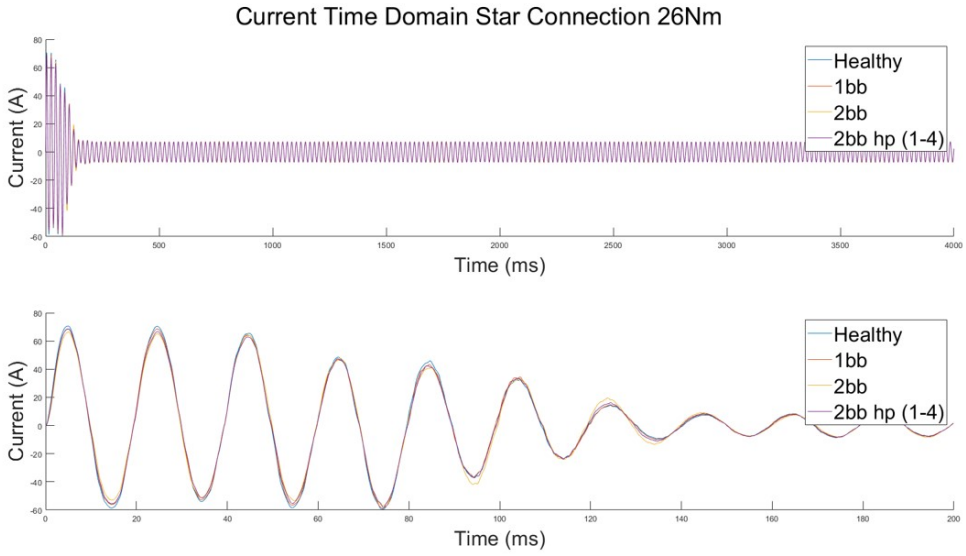

Figure 4.8: Star current time domain in the different proposed cases: healthy, 1 broken bar, 2 adjacent broken bars and 2 non-adjacent broken bars (1-4)

Thanks to the zoomed in graphs, it can be seen how the motor takes longer to compensate for the losses produced by two adjacent broken bars compared to two non-adjacent ones. This process may be due to the fact that this fault produces a greater interruption in the electrical continuity. This is not a very critical fault due to its low probability of occurrence.

MCSA

This analysis, as mentioned above, is used as a preventive method against the impact that the broken bars can make. This method consists on the elaboration of a frequency spectrum of the stator's current, in order to analyse the different side-bands which appear in function of the breakage of the rotors bars. The MCSA results are represented in figures 4.9 and 4.11, followed by the amplitudes of the main broken bar fault signature at $f_S - 2sf_S$ (Table 4.1).

When interpreting the data obtained by the MCSA, it is necessary to observe the two side bands present in the analysis. Firstly, the right-band is produced by the speed ripple and its analysis is normally associated with the inertia of the electromechanical system. In the case of this motor, it is not analysed in detail because of its close similarity to the left-band. Secondly, the left-band provides information on the rotor breaks and the impact they have

on the performance of the motor. Depending on their amplitude, it can be determined how much damage they cause.

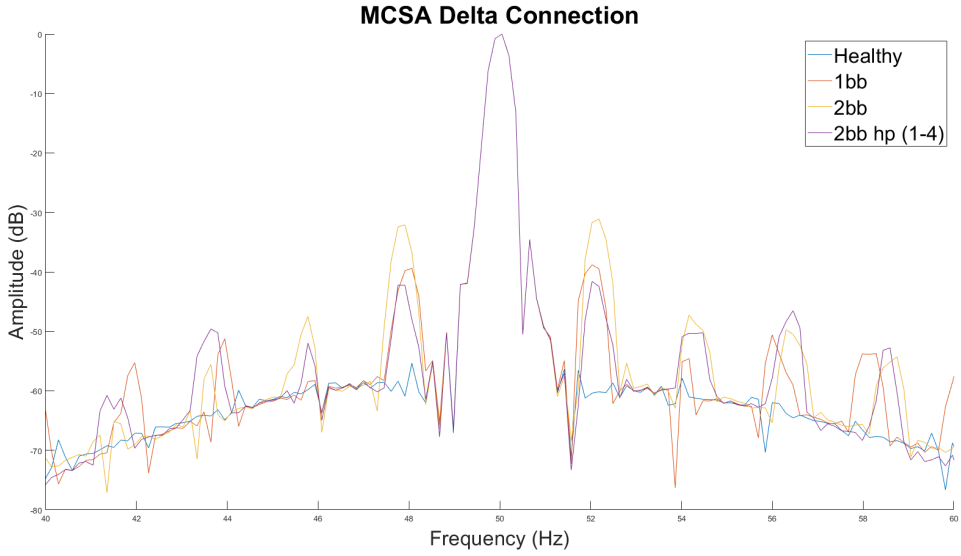

Figure 4.9: MCSA in delta connection under healthy and faulty conditions

Cases	$f_S - 2sf_S$
Healthy	-55.3435 dB
1 broken bar	-39.3834 dB
2 adjacent broken bar	**-32.0771 dB**
1 non-adjacent broken bar (1-4)	-42.221 dB

Table 4.1: MCSA Left side band in delta connection under healthy and faulty conditions

The MCSA results obtained illustrate one of the main disadvantages of this analysis, the masking of faults. In some faulty cases, the current spectrograms results in weak fault signatures with weaker amplitudes than those produced by the breakage of a single bar. Using an hypothetical case where a threshold of -40 dB is set, the failure of two non-adjacent breaks would not be identified and be classified as healthy. This masking is observed more clearly as the breakage of non-adjacent bars is performed with more bars as separation, reaching the case of the breakage of bars 1-5, where the results obtained resemble those of a healthy model.

These results are most visible in the graphs shown in the figure, where the MCSA results of the healthy model are compared with those of the failed models by two non-adjacent bars. It can be seen that breaking bars 1-3 results in a higher rupture than breaking bars 1-5. The

comparisons have been made in isolation between the healthy model and a failed model in order to obtain more clarity in the comparisons.

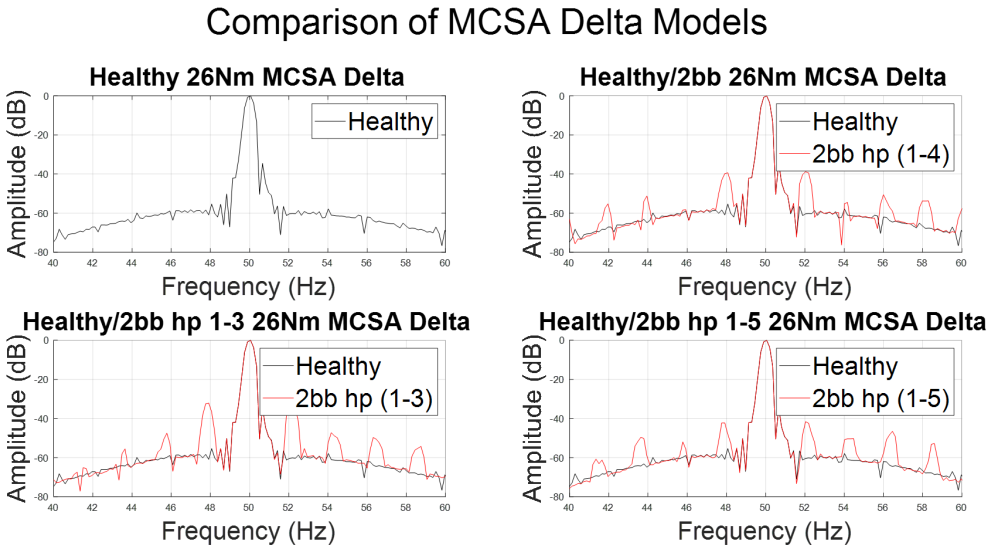

Figure 4.10: Delta MCSA current's spectrograms comparison in different proposed cases: healthy, 1 broken bar, 2 adjacent broken bars and 2 non-adjacent broken bars (1-4)

This behaviour observed with the delta connection is also observed in a similar way with the star connection, as it is seen in Figures 4.11 and 4.12.

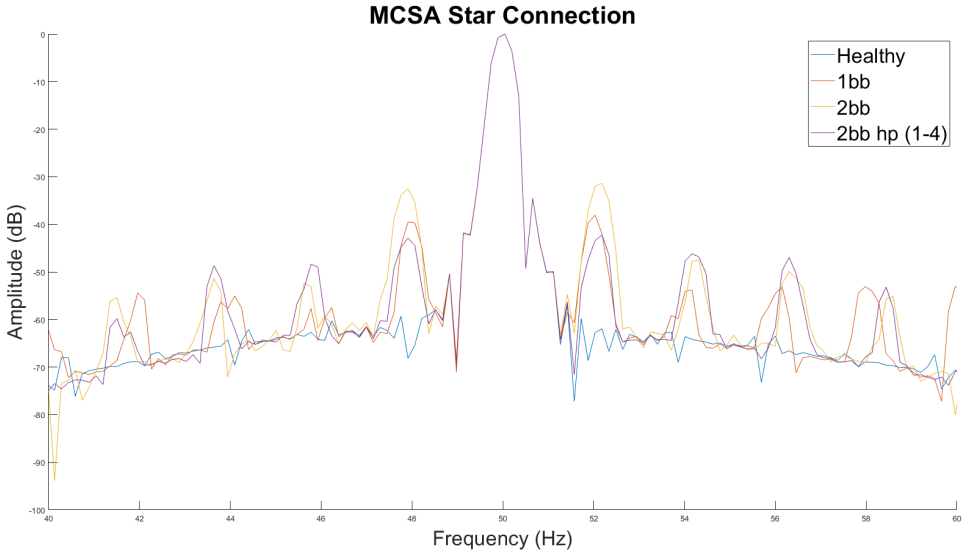

Figure 4.11: MCSA in star connection under healthy and faulty conditions

It can be seen that there are no pronounced frequency peaks in the harmonics, unlike with the delta connection. This difference may be due to the model, or to the inductive reactance of the windings, where in the delta connection, as it has a higher current, more noticeable transients may be produced.

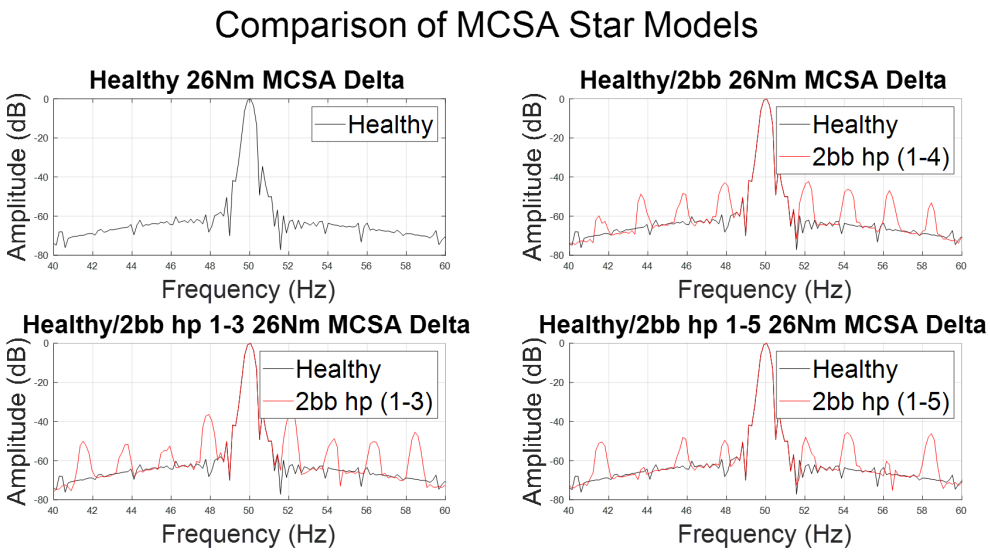

Figure 4.12: Star MCSA current's spectrograms comparison in different proposed cases: healthy, 1 broken bar, 2 adjacent broken bars and 2 non-adjacent broken bars (1-4)

Current STFT

Due to the high speed of the transient state, it does not generate enough information to be able to analyse the current during the transient state. Because of this, the moment of inertia has been increased to a value of 0.4 $Kg.m^2$, where as the following equation dictates, this parameter is strongly related to the angular velocity and therefore to the transient time.

$$T_{en} = J\frac{dw}{dt} + T_n \tag{4.3}$$

where the therm J refers to the combination between the moment of inertia of the rotor and the load it drives, T_n denotes the load torque that the motor needs to overcome to perform its work, T_en means the mechanical torque that the motor needs to generate and $\frac{dw}{dt}$ refers to how the angular speed changes along the time, in other words, angular acceleration.

For this analysis, the Short-Time Fourier Transform (STFT) has been employed to process the stator current data for all motor cases under study, thereby generating the corresponding spectrograms. In order to synthesise these spectrograms and to achieve a better relationship between time resolution and spectral resolution, the Kaiser window has been used. To optimise the filter utilised by this window, a beta parameter of 6.95, an overlap of 62% and a window length of 2348 samples has been used. The signal under study consists of 20,000 samples, sampled at a frequency of 10,000 Hz.

In this transient analysis, the spectrogram of the healthy motor (Figure 4.13) clearly shows the fundamental frequency as well as the fifth harmonic, who provides information about common non-linearities, such as small wave distortions or slight magnetic saturation.

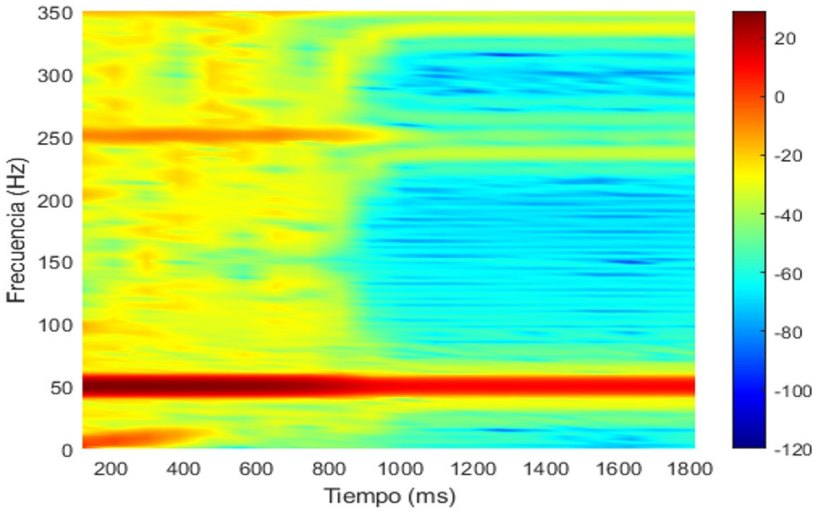

Figure 4.13: STFT current spectrogram of studied IM with healthy conditions during the start-up transient.

Furthermore, the spectrogram reveals the presence of two side bands surrounding the fundamental frequency. These sidebands, $f_{sb} = (1 \pm s) f_s$, do not remain at a constant frequency. On the contrary, as they depend on the motor's slip, they follow a trajectory that try to approach the fundamental frequency over time. The origin of these trajectories takes place at 100Hz and 0Hz at the initiation of the start-up, due to the fact that it is at this instant of time where the slip is 1, as the motor is not working.

However, although these characteristics can also be observed in the faulty models, additional harmonic trajectories emerge when bar breaks occur, like the characteristic V-shaped pattern below the fundamental frequency, $f = (1 - 2s) f_s$, becoming more evident while as much impact is generated by the breakages. As its seen in Figure 4.14, some trajectories can begin to be shown, such as $f = (1 + 2s) f_s$ or $f = (5 + 3s) f_s$.

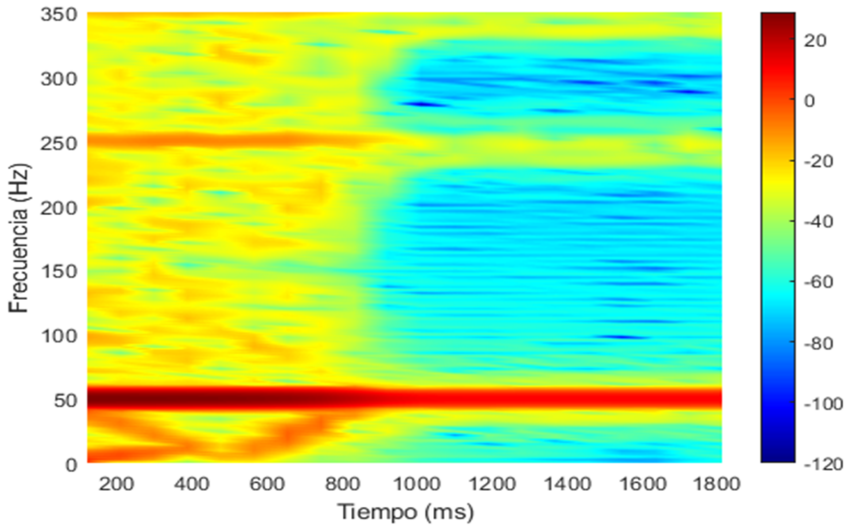

Figure 4.14: STFT current spectrogram of studied IM with 1 broken bar during the start-up transient.

These trajectories increase their amplitude considerably in the case of the rupture of two adjacent bars, as shown in the Figure 4.15. On the contrary, this increment is not related to the number of breaks, but to the proximity of the break, because as it can be seen in the Figure 4.16, the trajectories with two non-adjacent broken bars are more pronounced than with one break but less visible than with two. These results provide crucial information for the diagnosis of real motors. The behaviour of these inherent manufacturing anomalies indicates how different variations of the faults can give very similar results, leading to an increased risk of misdiagnosis, even in transient analysis. These misdiagnoses can result in the failure to perform necessary maintenance, thus causing a decrease in motor life.

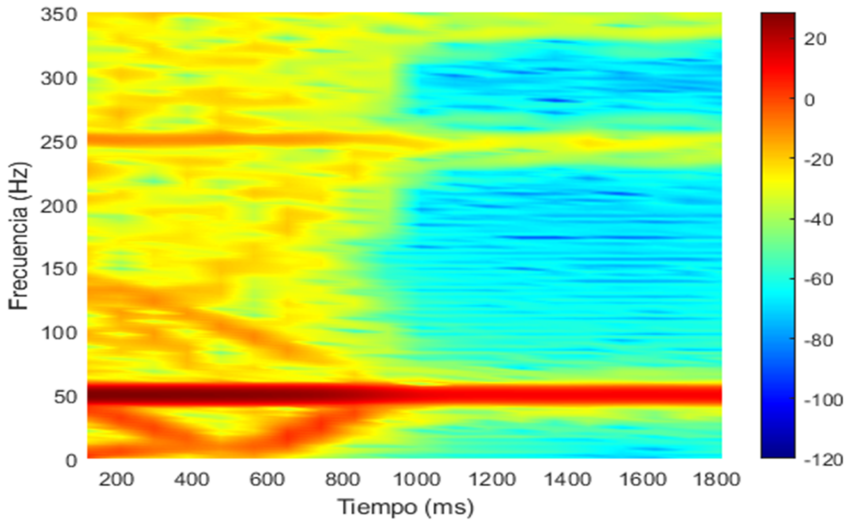

Figure 4.15: STFT current spectrogram of studied IM with 2 adjacent broken bar during the start-up transient.

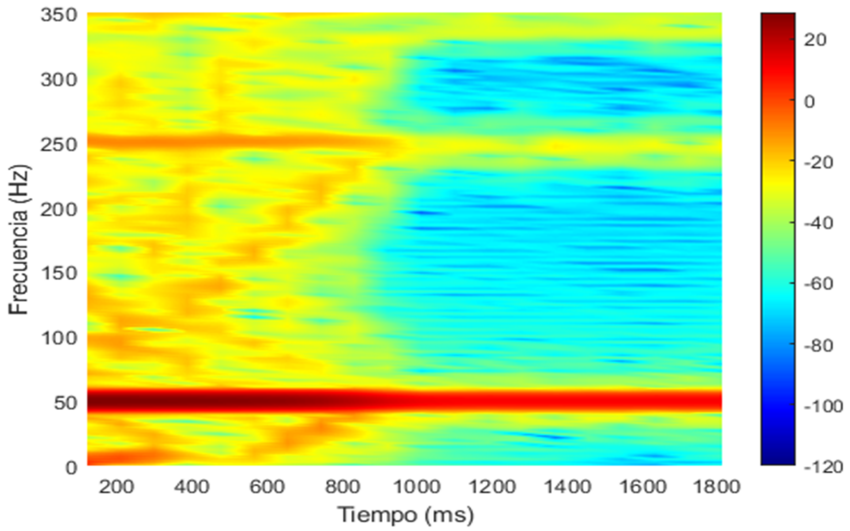

Figure 4.16: STFT current spectrogram of studied IM with 2 non-adjacent broken bar during the start-up transient.

The results obtained in star connection (Figure 4.17) show a similar behaviour to those obtained in delta. In these STFTs, the different harmonic trajectories mentioned above can be observed more clearly, as in the case of the healthy model, where the right sideband is more clearly defined. It can also be observed how in star the fifth harmonic extends for a longer time, compared to delta, remaining present also in the steady state.

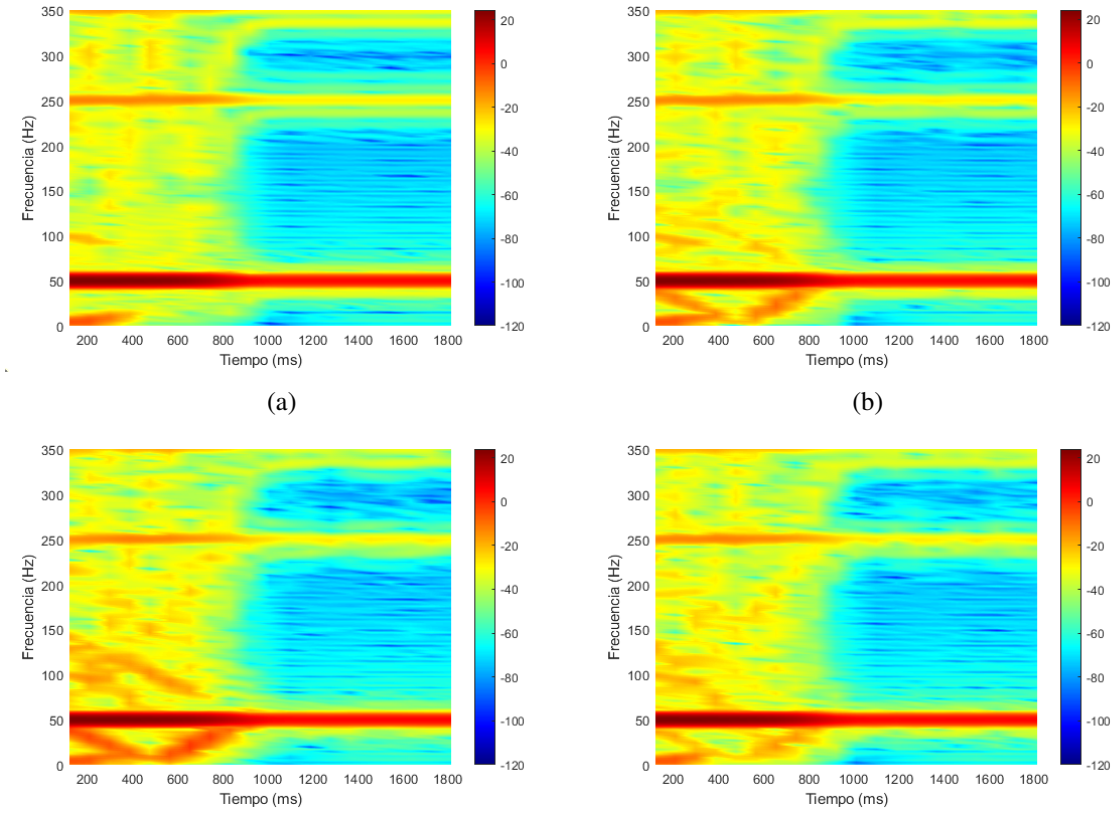

Figure 4.17: Star STFT's current spectrograms in different proposed cases: 4.17(a) healthy, 4.17(b) 1 broken bar, 4.17(c) 2 adjacent broken bars and 4.17(d) 2 non-adjacent broken bars (1-4)

4.5 Torque Analysis

Steady State

As with the MCSA analysis, the results provided by a stationary analysis of the machine torque allow the impact of bar breakage on the machine's operation to be identified. Analysing this torque it can be seen how the side bands harmonics are more prominent in failed models compared to the healthy model. The amplitudes of these harmonics (Table 4.2) determine the impact and damage these failures will have on engine performance. As it can be seen in Figure 4.18, these signals are weak and do not reach or exceed the theoretical threshold used in the rest of the analysis. This fact causes that through this analysis, the failed models pass as healthy, giving rise to erroneous diagnoses.

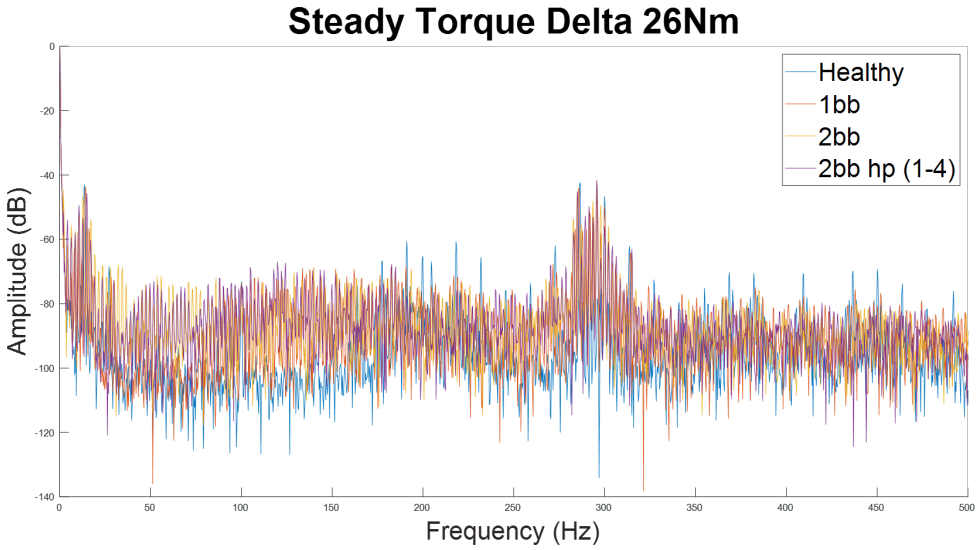

Figure 4.18: Steady state torque in delta connection under healthy and faulty simulated cases

Cases	$4sf_s$	$8sf_s$
Healthy	-79.2314 dB	-74.1616 dB
1 broken bar	-69.8322 dB	-65.4554 dB
2 adjacent broken bar	**-55.7401 dB**	**-46.482 dB**
2 non-adjacent broken bar (1-4)	-57.3971 dB	-53.415 dB

Table 4.2: Torque faulty signature in delta connection under healthy and faulty conditions

In the figure 4.18, the presence of the sixth harmonic (250+50) in the spectrogram can be clearly observed. This harmonic is of the sixth order and is typical in three-phase systems such as induction motors. It serves as a reflection of normal motor behaviour as well as to

indicate the presence of faults or damage to the motor. When a bus-bar break occurs, certain sidebands () are generated around the harmonic, indicating a fault in the motor. Although not clearly visible on the spectrogram, a significant increase in the amplitude of this harmonic is usually also indicative of failure. It is in this way that torque analysis is a critical step in the diagnosis of IM.

The behaviour of the failures is very similar to that observed in the MCSA results. When non-adjacent bars break, the impact of this failure decreases the further apart the bars are. This behaviour can also be observed in the star-connected motor (Figure 4.19).

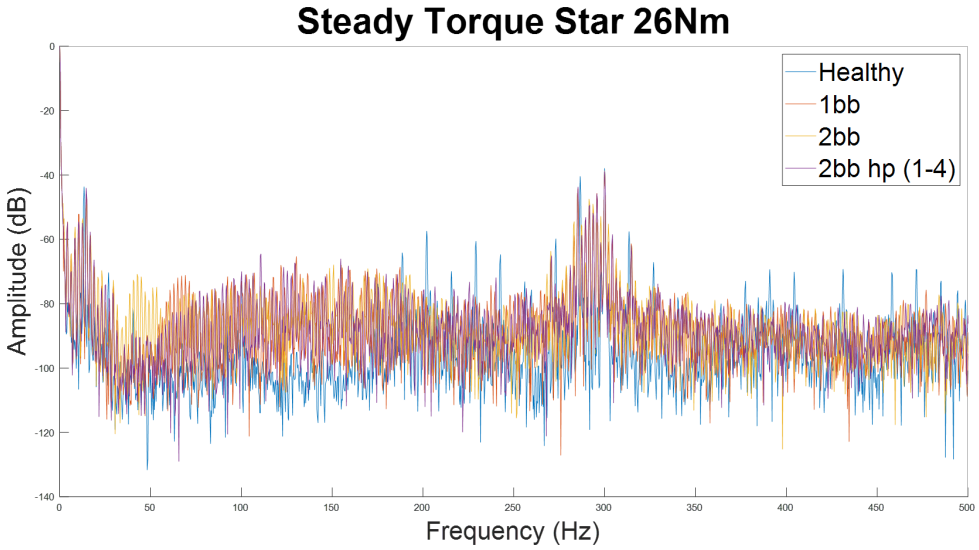

Figure 4.19: Steady state torque in star connection under healthy and faulty simulated cases

These results are most visible in the graphs shown in the Figures 4.20 and 4.21, where the torque results of the healthy model are compared with those of the failed models. The comparisons have been made in isolation between the healthy model and a failed model in order to obtain more clarity in the comparisons. Here it can observe more closely the alteration in the sixth harmonic due to the faults in the engine, as well as the sidebands that these faults also originate around the fundamental frequency.

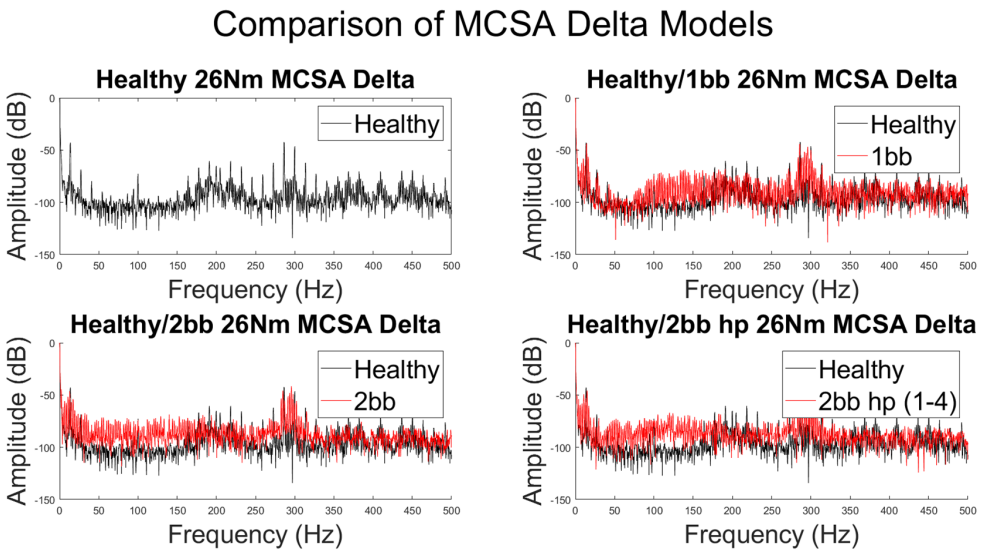

Figure 4.20: Delta torque's spectrograms comparison in different proposed cases: healthy, 1 broken bar, 2 adjacent broken bars and 2 non-adjacent broken bars (1-4)

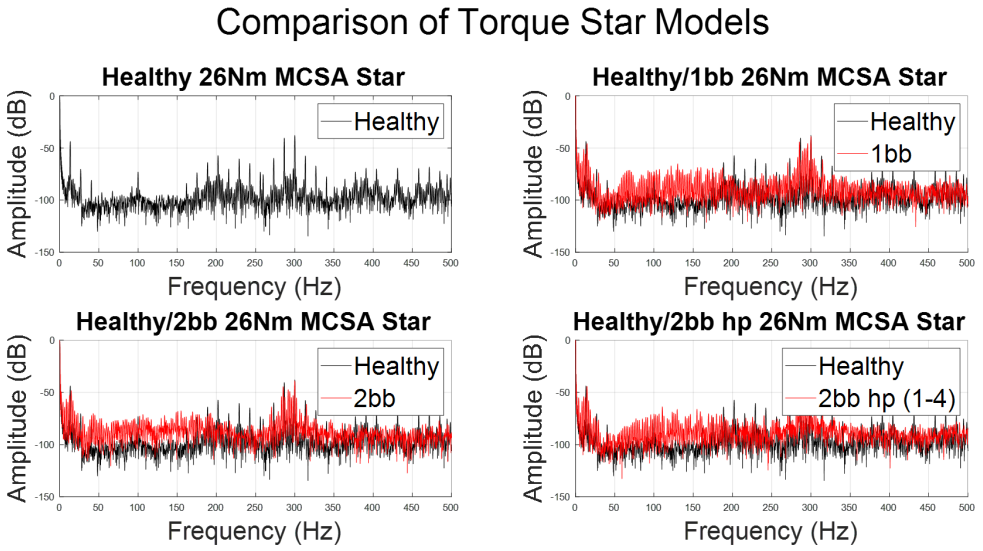

Figure 4.21: Star torque's spectrograms comparison in different proposed cases: healthy, 1 broken bar, 2 adjacent broken bars and 2 non-adjacent broken bars (1-4)

Transient

Analysing the transient torque of the motor (Figure 4.22), it can be clearly observed the presence of a continuous component at 0Hz regardless of whether the model is healthy or faulty. This continuous component refers to the average value of the torque provided by the motor. Its absence or alteration can mean several things, from the signal being leaked to rotor damage causing a loss of torque, making the torque oscillating. This component thus serves as an indication of the performance of the motor.

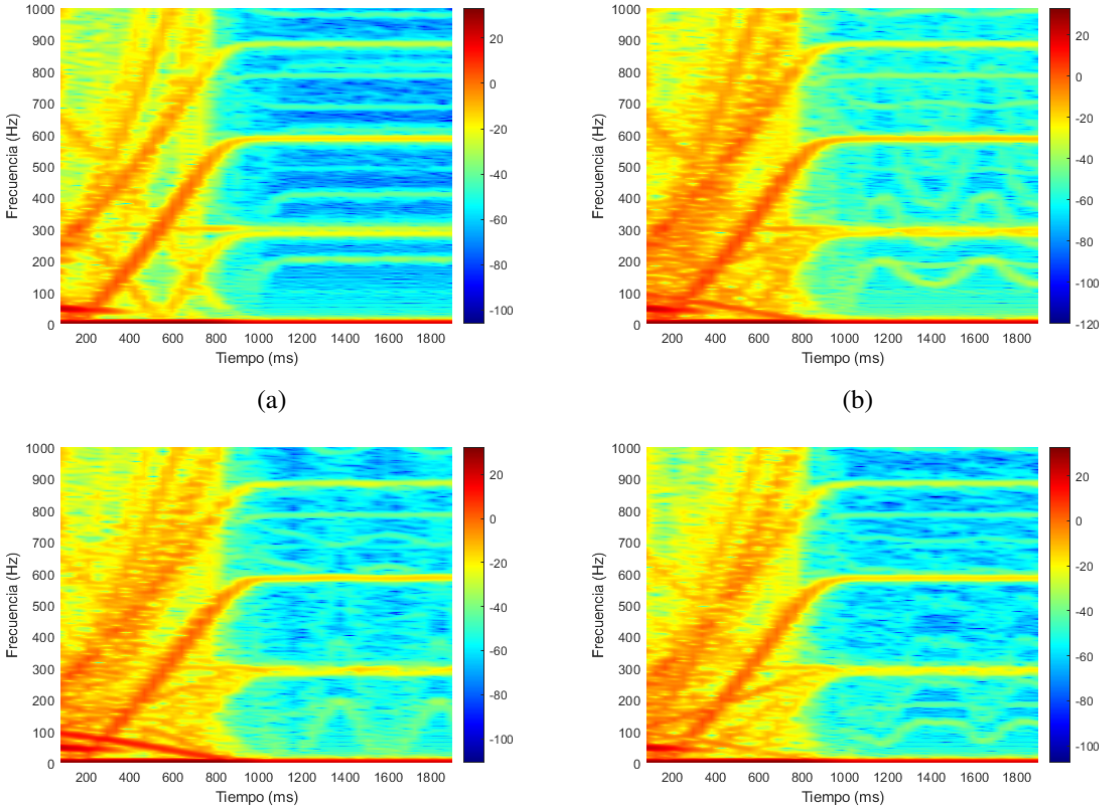

Figure 4.22: Delta STFT's torque spectrograms in different proposed cases: 4.22(a) healthy, 4.22(b) 1 broken bar, 4.22(c) 2 adjacent broken bars and 4.22(d) 2 non-adjacent broken bars (1-4)

This DC component is not the only one in the motor, more DC components can also be observed at frequencies 300, 600 and 900 Hz. These harmonics are generated periodically at frequency multiplies of 300 Hz, becoming less evident the further away they are from the fundamental frequency (50 Hz). This relationship indicates that a single periodic source is responsible for generating these harmonics, their origin being the magnetic saturation of the

motor or non-linearities caused by the hysteresis cycle. These trajectories, $f = (18 - 12s)f_s$ and $f = (12 - 12s)f_s$, can be observed regardless of the model simulated.

In the healthy model under nominal conditions (Figure 4.22(a)), certain harmonic trajectories become evident, such as $f = (8s)f_s$.It is evident that these trajectories become increasingly deflected as the impact of the faults on the motor intensifies. In the event of a bar breakage (Figure 4.22(b)), the other trajectories are overshadowed by lateral bands that emerge around them. These sidebands originate primarily around the previously mentioned continuous components, increasing in amplitude significantly when two adjacent bars break.

At the moment of bar breakage, a harmonic trajectory around the fundamental frequency becomes more evident. This trajectory, $f = (1 - 1s)f_s$, is more pronounced when two adjacent bars break (Figure 4.22(c)). In contrast, when bars 1 and 4 break, the trajectory is less clear. Its origin lies in the loss of symmetry that occurs in the magnetic field of the rotor, which generates asymmetrical components in the magnetic flux.

An analysis of the results obtained for the failed models reveals the emergence of a specific phenomenon surrounding the second harmonic. When the asymmetries occur in the rotor, a sinusoidal trace is observed around the frequency 100 Hz, becoming more evident in the case of a single break, in contrast to two non-adjacent bars (Figure 4.22(d)). This sinusoidal modulation is attributed to a periodical failure of the motor. The initial occurrence of the phenomenon at 800 milliseconds can be attributed to the fact that at this precise moment, the velocity of the motor reaches the steady state.

As illustrated in Figure 4.23, the previously mentioned characteristics are also evident in the star connection. The primary distinction observed pertains to the break of a bar, where distortions and sidebands that emerge are less pronounced and possess reduced amplitude in comparison to the delta connection. Furthermore, an increased perceptibility of the sinusoidal modulations is evident in the various faulty simulations. The main cause of this phenomenon is the voltage applied to the motor. In star, the use of a lower phase voltage, makes the spectrograms produced tend to present less harmonic distortion, making the modulations at low frequencies more evident. In the contrary, the delta connection exhibits stronger harmonics that can generate a masking of the modulations, making the fine diagnosis of the motor more difficult.

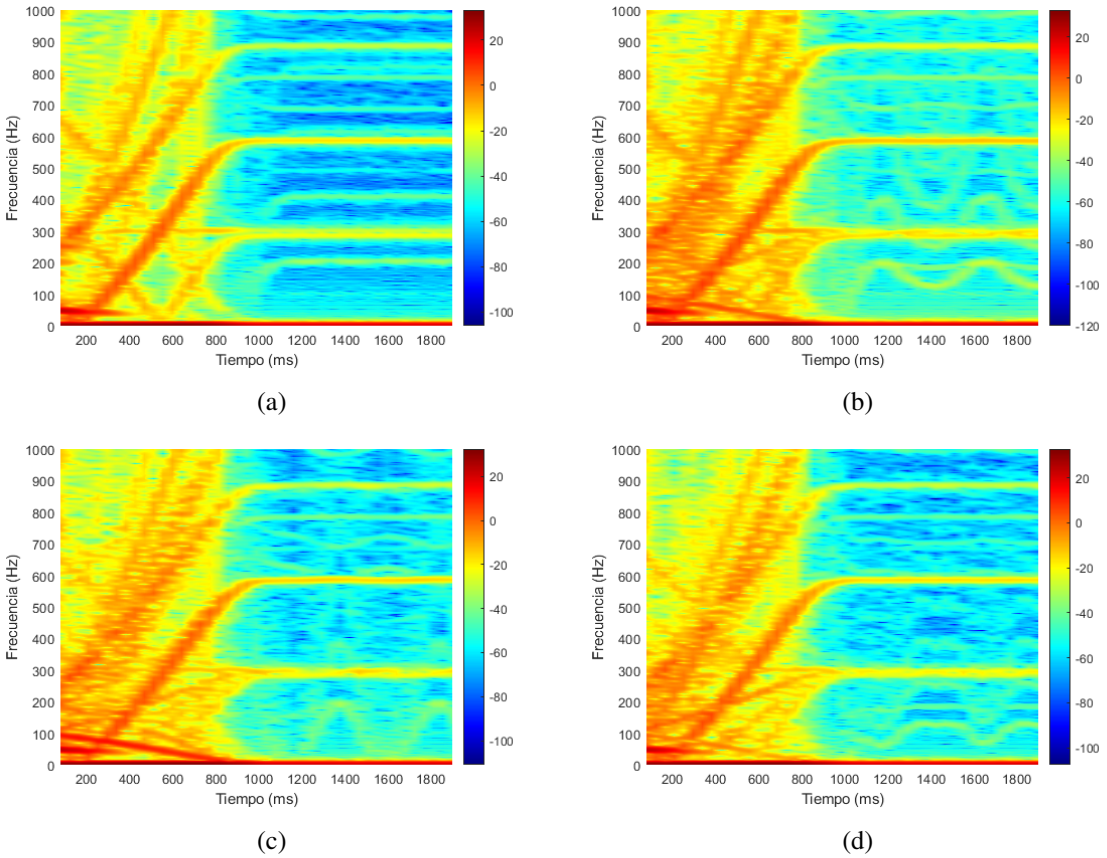

Figure 4.23: Star STFT torque spectrograms in different proposed cases: 4.22(a) healthy, 4.22(b) 1 broken bar, 4.22(c) 2 adjacent broken bars and 4.22(d) 2 non-adjacent broken bars (1-4)

4.6 SFSA

Steady State

The stray flux analysis provides similar results to those obtained by stator current analysis (MCSA), exhibiting equivalent signatures. Being a complementary analysis, the results obtained after using the FFT provide supplementary signatures that are directly related to the rotor speed. These signatures allow to overcome and clarify possible potential misdiagnoses. The results obtained are the consequence of processing the induced voltage information in one of the sensors located around the stator and applying FFT to it, thus creating the spectrograms necessary for the analysis.

As shown in the spectrogram of Figure 4.24, which shows the SFSA of all the simulated cases in delta connection, the most significant signatures (Table 4.3) are those described by the equation 4.4, which allows to calculate the frequency of the harmonics that will be affected by the electrical faults in the rotor. As numerous recent studies have shown, rotor electrical faults amplify the harmonics closely linked to the mechanical speed of the rotor, making it possible to enhance early detection of anomalies by studying them.

$$f_{bb3} = \left[n \pm m \frac{(1-s)}{p} \right] f_s \tag{4.4}$$

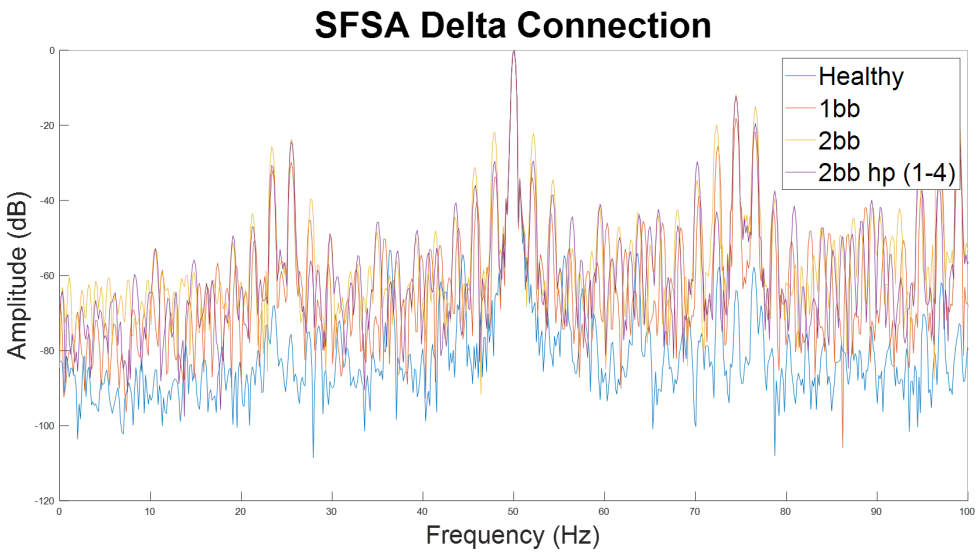

Figure 4.24: Delta SFSA results in the different proposed cases: healthy, 1 broken bar, 2 adjacent broken bars and 2 non-adjacent broken bars (1-4)

Simulated Cases	$1 - 2\frac{1-s}{p} f_s$	$1 + 2\frac{1-s}{p} f_s$
Healthy	-75.633 dB	-63.935 dB
1 broken bar	-29.7892 dB	-18.1539 dB
2 broken bars (adj)	**-23.7202 dB**	**-11.7617 dB**
2 broken bars (1-4)	-24.39 dB	-12.2725 dB

Table 4.3: SFSA signature's amplitudes in delta connection under healthy and faulty conditions

As demonstrated in Table 4.3, it is evident that the longest harmonic corresponds at all times to the condition of two adjacent broken bars. It is important to note that, in the event of two non-adjacent bars breaking, there is also a considerable increase in the harmonic, which is slightly lower. This behaviour enables the diagnosis that, although either failure conditions are damaging and have a significant impact on the motor, the adjacent broken bars have the most pronounced effect on the machine.

Furthermore, the spectrogram demonstrates the emergence of sidebands surrounding the fundamental frequency (50 Hz) in the simulations of fault conditions.The formation of these bands is attributed to modulation resulting from internal defects in the motor. The intensity of these sidebands depends on the type of fault and its impact, resulting in more anomalous or wider bands, depending on the modulation these faults generate. Their study allows the identification of the defect and its location.

These results also show a general increase in spectral amplitude under fault conditions. This effect is caused by the loss of symmetry in the magnetic field due to the breakage of the bars. Due to this asymmetry, the magnetic field is not evenly distributed, causing periodic and irregular fluctuations in the stray magnetic flux.

In order to be able to observe these characteristics more closely, comparative graphs have been made where the model is studied in healthy conditions with each failure caused, so that the impact and signatures of each defect can be studied separately. This comparison is illustrated in Figure 4.25. It is here that it can be seen in more detail how under the condition of a breakage of two rotor bars, either adjacent or non-adjacent, there is a considerable increase in the spectral amplitude in contrast with the healthy model or with the condition of a single break. It is also observable that as the severity of the failure increases, the sidebands intensify, making the appearance of spectral noise more noticeable as well.

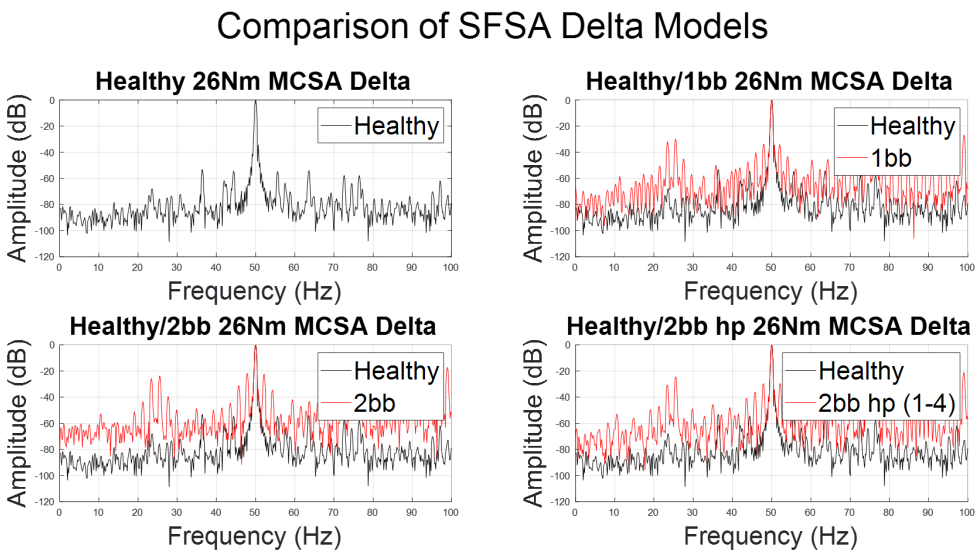

Figure 4.25: Delta SFSA's spectrograms comparison in different proposed cases: healthy, 1 broken bar, 2 adjacent broken bars and 2 non-adjacent broken bars (1-4)

All these characteristics are also observable in the star connection shown in figures 4.26 and 4.27. In this type of connection it is possible to appreciate how, unlike in delta, the spectrum generated by the fault conditions turns out to be less noisy, which makes it easier to detect subtle changes or more imperceptible harmonics. It is also possible to observe that in this type of connection, the spectral amplitude is slightly higher than that observed in delta. This effect is more noticeable and can be better appreciated in Figure 4.27, where the sidebands around the fundamental frequency are slightly increased with respect to those observed in Figure 4.25.

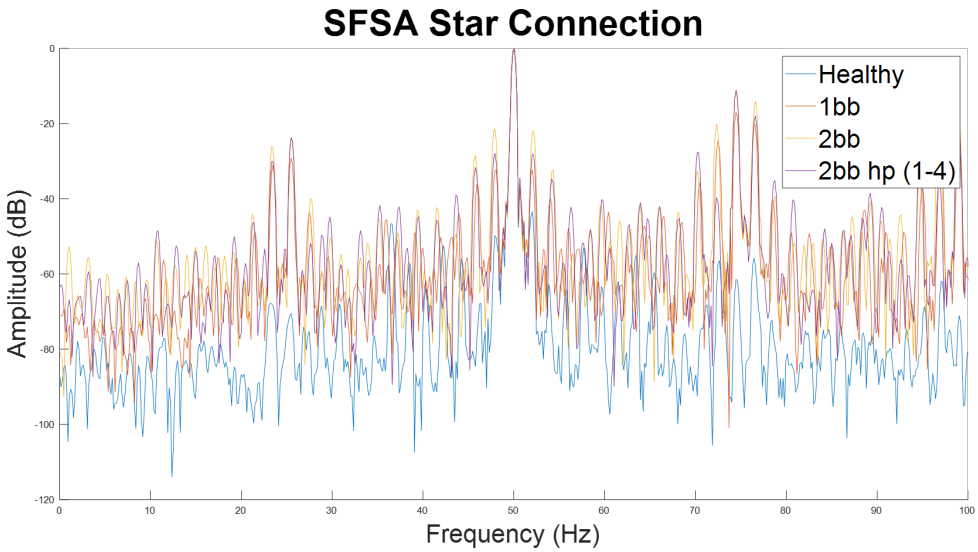

Figure 4.26: Star SFSA results in the different proposed cases: healthy, 1 broken bar, 2 adjacent broken bars and 2 non-adjacent broken bars (1-4)

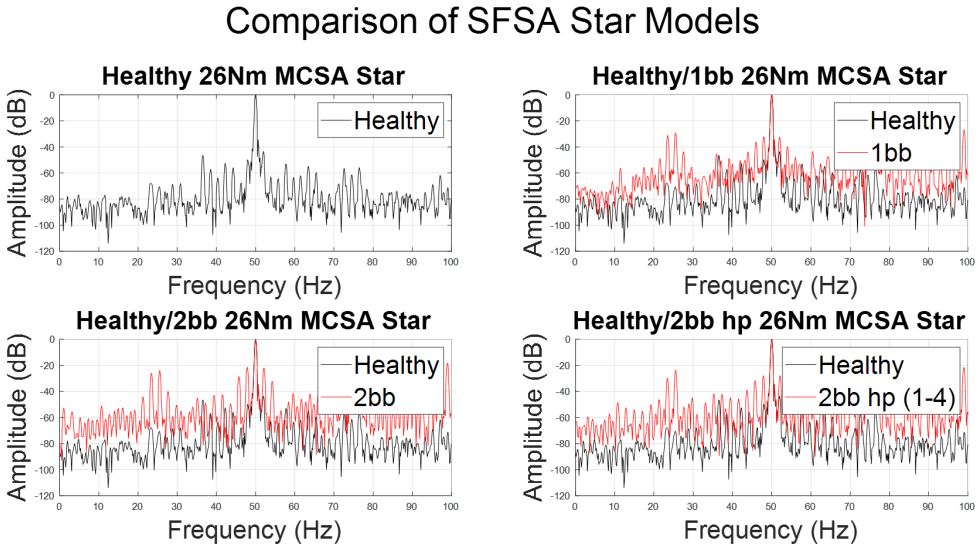

Figure 4.27: Star SFSA's spectrograms comparison in different proposed cases: healthy, 1 broken bar, 2 adjacent broken bars and 2 non-adjacent broken bars (1-4)

Transient State

Analysing the stray flux of the motor under healthy operating conditions (Figure 4.28), it can be seen how the provided STFT actively exhibits defined frequencies (50,150,250,...), thus reporting a periodical modulation on odd harmonics. It is also possible to observe how there are certain green and light blue areas along the spectrogram, most of which are clustered

together during steady state operation. These zones are indicative of low amplitude and low electromagnetic noise. This feature allows a clean, predictable and harmonically ordered pattern to be established which will serve as a precedent for observing the effects of fault conditions on the motor.

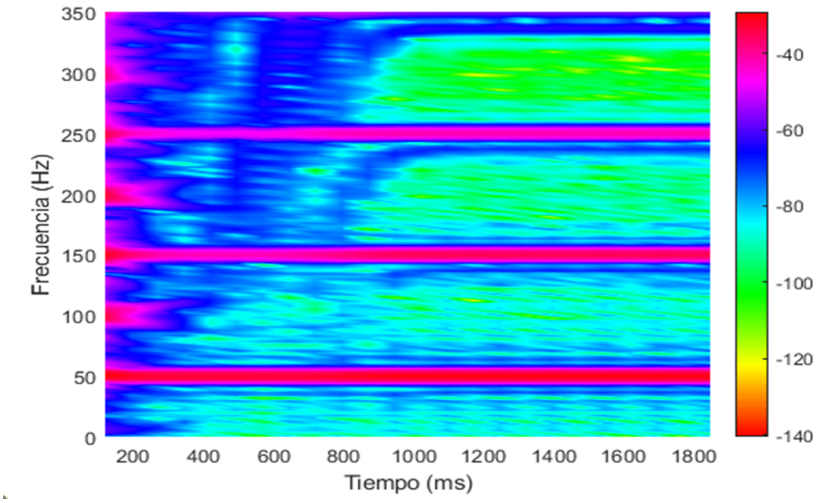

Figure 4.28: STFT SFSA spectrogram of studied IM with healthy conditions during the start-up transient.

At the moment when a single bar breaks (Figure 4.29), the STFT of the stray flux is greatly altered. These lie mainly in the appearance of a higher spectral content in the previously 'clean' bands. Around the even-order harmonics, there is a breakdown and reduction of uniformity compared to the healthy model, which is evidenced by the appearance of red and magenta shades. This wave modulation and creation of sidebands serves as an indication of the appearance of an anomaly in the motor capable of altering the symmetry of the magnetic field.

These alterations are more evident in the case of breakage of two adjacent bars (Figure 4.30), where the modulation is greater. This suggests that although both single and double breakage have a major impact on the motor, the second condition poses a slightly greater risk to the life of the motor.

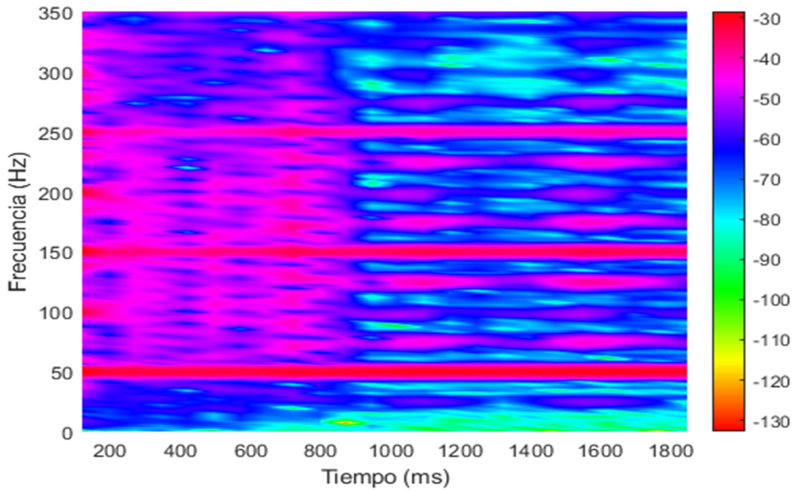

Figure 4.29: STFT SFSA spectrogram of studied IM with 1 broken bar during the start-up transient.

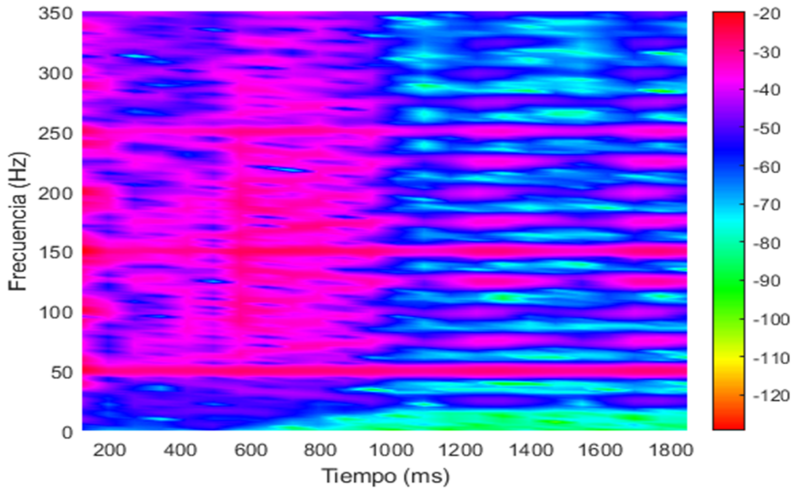

Figure 4.30: STFT SFSA spectrogram of studied IM with 2 adjacent broken bars during the start-up transient.

This modulation is not so great in the case of the breakage of two adjacent bars (Figure 4.31). On the other hand, the disintegration produced is less evident, allowing a better observation of the lateral bands produced by the breakage. These sidebands originate mainly from the odd-order harmonics. This is due to the fact that these harmonics are responsible for generating the magnetic fields that interact with the rotor.

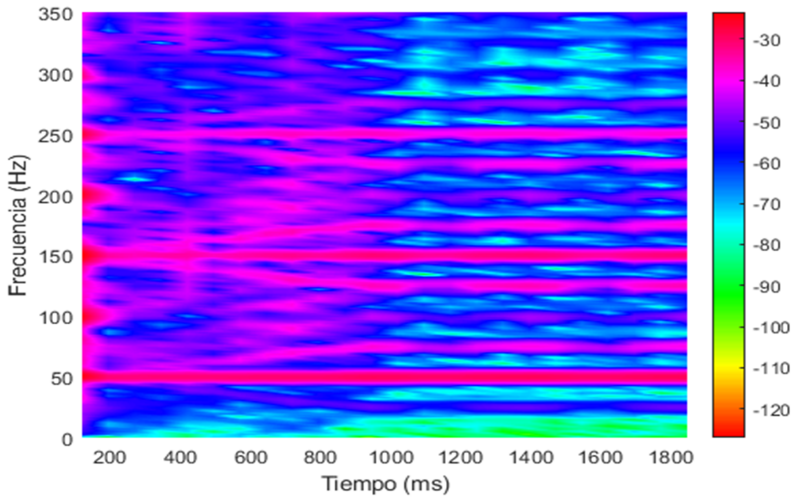

Figure 4.31: STFT SFSA spectrogram of studied IM with 2 non-adjacent broken bars during the start-up transient.

As expected, the results obtained in the star connection (Figure 4.32) differ minimally from those obtained in the delta connection.

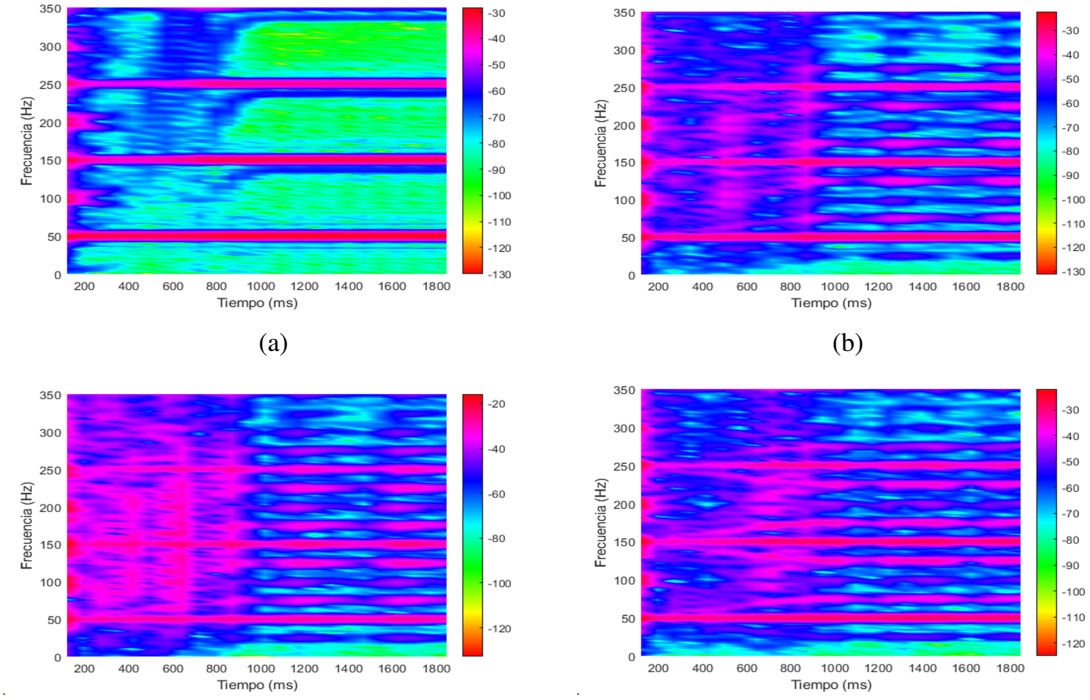

Figure 4.32: Star STFT SFSA spectrograms in different proposed cases: 4.32(a) healthy, 4.32(b) 1 broken bar, 4.32(c) 2 adjacent broken bars and 4.32(d) 2 non-adjacent broken bars (1-4)

The most noticeable differences that can be seen are in the case of a single bar break, where, as it can be seen in the Figure 4.32(b), the dispersion that occurs in the harmonics is smaller, and the sidebands that appear around them are less evident. This reduction in wave modulation is a result of the reduction in electromagnetic noise in the star connection compared to the delta, due to the lower voltage required in this type of connection.

Chapter 5

CONCLUSION AND FUTURE WORK

5.1 Conclusions

In this thesis it has been demonstrated how the combination of electromagnetic modelling and signal analysis constitutes an effective and non-invasive method for the detection of faults in induction motors, with more detail on squirrel cage motors. By means of 2D simulation in Simcenter MAGNET, together with finite element analysis (FEA), it has been possible to identify clear variations in the current, torque and stray flux signatures caused by the different fault conditions proposed in the rotor bars.

Thanks to the use of different diagnostic techniques such as SFSA and MCSA it has been possible to effectively and reliably differentiate healthy motors from those with one or more broken bars, both in the star and delta configurations. These techniques have made it possible to observe how the signatures and spectral responses of the results obtained vary from one case to another depending on the severity of the fault and its location, making it easier not only to detect it but also to estimate its impact.

The results obtained in the healthy models show errors of less than 10% with respect to the theoretically provided data, which supports the accuracy of the approach used. Furthermore, this study underlines the importance of electromagnetic analysis in the industrial field as a preventive tool, capable of detecting faults before they cause severe damage to the motor and contributing to the increase of the motor's lifetime.

5.2 Future Work

Thanks to the results obtained throughout the thesis, many avenues are open for future research. Firstly, the extension of these analyses and simulations to induction motors of different powers, sizes and materials will allow the validation of these techniques and their generalisation to a wider industrial spectrum. Additionally, these techniques can include a thermal analysis of the motor, in order to increase their robustness and allow a better understanding of thermal effects such as expansion, thermal radiation, ...

Lately, a key addition to the studies carried out would be the automation of these analyses in real time. This addition would be implemented through the use of programmable logic controllers (PLCs) and controllers that would analyse the operation of the motor throughout its performance, together with the addition of artificial intelligences that would identify

differences and failures and classify them.

Finally, an interesting addition to this study would be the validation of the simulations with examples of physical motors, in order to verify the results and refine the electromagnetic models. These additions would enhance the development of the electromagnetic analysis of the motors making it more reliable and efficient.

BIBLIOGRAPHY

[1] S. E. Moya, "Efficient electric motors for the industrial sector," M.S. thesis, Carlos III University of Madrid, Feb. 2015.

[2] N. G. Ozcelik, M. Imeryuz, U. E. Dogru, and L. T. Ergene, "Synchronous reluctance motor vs. induction motor at low-power industrial applications: Design and comparison," *Energies*, Jun. 2019. DOI: 10.3390/en12112190.

[3] S.S.Bhavikatti, *Finite Element Analysis*. New Age International, 2005, ISBN: 978-81-224-2524-6.

[4] J.-M. Jin, *The Finite Method in Electromagnetics*. John Wiley & Sons, 2015, ISBN: 978-1-118-57136-1.

[5] F. Mora, *Máquinas Eléctricas*. Concepción Fernández Madrid, 2015, ch. Asynchronous machines.

[6] C. Liu, "Emerging electric machines and drives — an overview," in *IEEE Transactions on Energy Conversion*, 2018.

[7] *Electromagnetism*. [Online]. Available: https://electromagnetismoluz2017.wordpress.com/2017/10/13/electromagnetismo/.

[8] M. Á. Rodríquez Pozueta, *Máquinas Eléctricas I G862*. Universidad de Cantabria (España), 2015.

[9] M. I. of Theconologies, "Faraday's law of induction," Chapter 10.

[10] S. Plotnikov, "Determination of eddy current losses and hysteresis losses in magnetic circuits of electrical machines," *Izmeritel'naya Tekhnika*, Jan. 2020. DOI: 10.32446/0368-1025it.2020-11-54-58.

[11] K. Yamazaki and S. Kokubo, "Induction motor analysis by considering hysteresis loops in stator and rotor," *IEEE Transactions on Magnetics*, Mar. 2021. DOI: 10.1109/TMAG.2021.3068131.

[12] *Transformer equivalent circuit*. [Online]. Available: https://ingenieriaelectricafravedsa.blogspot.com/2014/12/circuito-equivalente-transformador.html.

[13] M. P. Donsión, *Synchronous machines*. Vigo University, 2021.

[14] S. J. Chapman, *Electric Machinery Fundamentals*. Elizabeth A. Jones, 1991.

[15] *Three-phase asynchronous motor types and operation*, OSWOS. [Online]. Available: https://oswos.com/es/motor-asincrono/#:~:text=Existen%20dos%20tipos%20diferentes%20de,ardilla%20y%20de%20anillo%20colector..

[16] E. C. Valencia Diego Fernandez; Quispe, "Methodology for estimating the influence of voltage harmonics on efficiency and power factor of three-phase induction motors," in *Power Electronics and Power Quality Applications (PEPQA)*, 2013.

[17] *Losses in a induction motor – power stages in asynchronous motor*, Electrical Technology. [Online]. Available: https://www.electricaltechnology.org/2022/07/power-stages-losses-induction-motor.html.

[18] J. Chen, Y. Du, H. Zhan, K. Zhou, and Y. Sun, "Comparative study of short circuits and demagnetization in delta, star, and hybrid winding connections for surface-mounted permanent magnet machines," *Machines*, Jun. 2024. DOI: 10.3390/machines12060401.

[19] J. A. Itajiba, C. A. C. Varnier, S. H. L. Cabral, *et al.*, "Experimental comparison of preferential vs. common delta connections for the star-delta starting of induction motors," *Energies*, Mar. 2021. DOI: 10.3390/en14051318.

[20] P. Lombard, "Determining end ring resistance and inductance of squirrel cage for induction motor with 2d and 3d computations," in *2016 XXII International Conference on Electrical Machines (ICEM)*, 2016.

[21] K. Yamazaki, "Approximated modeling of end-rings for electromagnetic field analysis of induction motors," in *IEEJ Transactions on Industry Applications*, Sep. 2001. DOI: 10.1541/ieejias.121.184.

[22] R. Khan, F. Yousof, R. A. Rahman, N. Azis, S. M. Al-Ameri, and A. Ali, "Broken rotor bar detection of three phase induction motor using frequency response analysis," *International Journal of Electrical and Computer Engineering (IJECE)*, Jan. 2025. DOI: 10.11591/ijece.v15i2.pp1289-1296.

[23] N. Mehala and R. Dahiya, "Motor current signature analysis and its applications in induction motor fault diagnosis," *International Journal Of Systems Applications, Engineering & Development*, Mar. 2008.

[24] J.-H. Jung, J.-J. Lee, and B.-H. Kwon, "Online diagnosis of induction motors using mcsa," *IEEE Transactions on Industrial Electronics*, Jan. 2007. DOI: 10.1109/TIE.2006.885131.

[25] G.-A. Capolino, J. Antonino-Daviu, and M. Riera-Guasp, "Modern diagnostics techniques for electrical machines, power electronics, and drives," *IEEE Transactions on Industrial Electronics*, Mar. 2015. DOI: 10.1109/TIE.2015.2391186.

[26] Y. Zhang, Z. Zeng, L. Yao, L. Qiao, L. Yin, and Y. Lu, "Modelling the rotating magnetic field with the skin effect," *International Journal of Applied Electromagnetics and Mechanics*, May 2017. DOI: 10.3233/JAE-160041.

[27] K. Gyftakis, "Electromagnetic analysis of induction motor faults and development of new diagnostic methods to detect them," Ph.D. dissertation, University of Patras, 2015.

[28] A. Sergakis, "Fault diagnosis in direct drive permanent magnet generators for offshore wind turbines," M.S. thesis, Technical university of Crete, 2024.

[29] F. H. Jufri, "Techno-economic analysis of slip ring motor replaced by standard squirrel cage induction motor with vsd," in *Journal of Physics Conference Series*, 2019. DOI: 10.1088/1742-6596/1402/3/033107.

[30] B. Noureddine and F. Benaida, "Diagnosis of broken rotor bars in six-phases squirrel cage induction motor," in *International Review of Electrical Engineering (IREE)*, Oct. 2022. DOI: 10.15866/iree.v17i5.21723.

[31] S. Zouzou, S. Khelif, N. Halem, and M. Sahraoui, "Analysis of induction motor with broken rotor bars using finite element method," *International Journal of Advance Engineering and Research Development*, Nov. 2011. DOI: 10.1109/EPECS.2011.6126821.